# REPORT DOCUMENTATION PAGE

*Form Approved*
*OMB No. 0704-0188*



| 1. REPORT DATE *(DD-MM-YYYY)* | 2. REPORT TYPE | 3. DATES COVERED *(From - To)* |
|---|---|---|
| 01/31/2012 | Final Technical report | 14-JUL-08 to 31-DEC-11 |

**4. TITLE AND SUBTITLE**
Using RANS calculations of turbulent kinetic energy to provide two point flow velocity correlations and surface pressure spectra

**5a. CONTRACT NUMBER**

**5b. GRANT NUMBER**
N00014-08-1-1122

**5c. PROGRAM ELEMENT NUMBER**

**6. AUTHOR(S)**
Glegg, Stewart

**5d. PROJECT NUMBER**

**5e. TASK NUMBER**

**5f. WORK UNIT NUMBER**

**7. PERFORMING ORGANIZATION NAME(S) AND ADDRESS(ES)**
Florida Atlantic University, 777 Glades Road, Boca Raton, FL33431

**8. PERFORMING ORGANIZATION REPORT NUMBER**

**9. SPONSORING/MONITORING AGENCY NAME(S) AND ADDRESS(ES)**
Office of Naval Research
875 North Randolph Street
Arlington
VA 22203-1995

**10. SPONSOR/MONITOR'S ACRONYM(S)**

**11. SPONSOR/MONITOR'S REPORT NUMBER(S)**

**12. DISTRIBUTION/AVAILABILITY STATEMENT**
Approved for public release



**13. SUPPLEMENTARY NOTES**

**14. ABSTRACT**
This report gives the results of a study that used the linearized Navier Stokes equations to model spectra in turbulent flows. The first part of the study considers two dimensional wakes and provides estimates of two point correlation functions and spectra from the distribution of turbulent kinetic energy in the flow. In the second part of the study a turbulent boundary layer in the vicinity of a forward facing step is analyzed and results are given for the velocity and surface pressure spectra. Results are also given for the Green's function and the sound radiation efficiency from turbulence close to a forward facing step. All results are compared with measurements obtained in a companion study at Virginia Tech.

**15. SUBJECT TERMS**
Hydroacoustics, boundary layers, turbulent flow, step flows

| 16. SECURITY CLASSIFICATION OF: | | | 17. LIMITATION OF ABSTRACT | 18. NUMBER OF PAGES | 19a. NAME OF RESPONSIBLE PERSON |
|---|---|---|---|---|---|
| a. REPORT | b. ABSTRACT | c. THIS PAGE | | | Glegg, Stewart |
| | | | | | 19b. TELEPHONE NUMBER *(Include area code)* |
| U | U | U | SAR | 57 | 561 297 2633 |

**FINAL REPORT**

# Using RANS calculations of turbulent kinetic energy to provide two point flow velocity correlations and surface pressure spectra

Contract Number : N00014-08-1-1122

Principal Investigator: Stewart A.L. Glegg

Dept. of Ocean and Mechanical Engineering
Florida Atlantic University
Boca Raton
FL 33431

Email: sglegg@fau.edu

January 2012

## Abstract

At the present time RANS calculations are widely used to determine the time averaged flow over bodies of arbitrary shape. However they do not provide the time dependent or spectral information required for the analysis of ship hull vibration, radiated noise and sonar performance. The objective of this study is to calculate space time velocity correlation functions and surface pressure wavenumber spectra in turbulent shear flows using information from time averaged RANS calculations, so that the details of high fidelity time averaged flow can be applied to hydroacoustic and structural vibration problems.

Recent advances in numerical techniques have resulted in efficient methods for calculating the Reynolds average statistics of the flow around most bodies. These calculations provide the mean, time invariant flow as well as the local turbulent kinetic energy and dissipation. However they provide no information on the higher order statistics or spectral content of the unsteady part of the flow. For many applications, especially those involving sound radiation, the local turbulent kinetic energy does not provide the information that is required. Ideally, a procedure for estimating the two point correlation function of the velocity fluctuations throughout the flow is needed.

In a recent study (Glegg *et al*(2010)), a method for calculating the surface pressure spectra below a turbulent boundary layer was developed which is based on the solution to the unsteady Euler equations and the Reynolds averaged Navier Stokes equations. It was shown that the unsteady velocity in a two dimensional linearized shear flow could be modeled using a distribution of vortex sheets. Each vortex sheet is convected at the local mean flow speed and its distribution can be used to specify all three components of the turbulent flow. The unsteady pressure, the two point velocity correlation functions, the turbulent kinetic energy and surface pressure wavenumber spectra was obtained directly from this equation in terms of the mean square value of the vortex sheet strength. Since RANS calculations give the distribution of turbulent kinetic energy in the flow, it was possible to invert the spatial distribution of turbulent kinetic energy to obtain the vortex sheet strength, and use the result to calculate all the statistical details of the unsteady flow. However, in this approach the specification of a turbulent energy spectrum that scales on the dissipation length scale was required and this is difficult to model universally.

In the first part of this study (see Part Ia) the linearized approach described above was extended to turbulent flows in two dimensional wakes described by the Orr Sommerfeld equations. Wake flows are more challenging than two dimensional boundary layers because the flow is continuously evolving in the downstream direction in a self similar manner. The theory was modified to allow for self similarity and the results were compared to experimental data of the two point velocity correlation functions in turbulent wakes (Devenport et al, 2001) with some success.

This approach is then used to predict rotor stator interaction noise that is caused by the wakes from upstream blades impinging on downstream stator vanes. The turbulence modeling developed in Part 1a is used in Part 1b to specify the turbulence in the inflow to the stators. Acoustic predictions show how the sound radiation is affected by the cutting angle of the wake relative to the leading edge of the blades.

In the second part of this report (Part II) the acoustic radiation from a turbulent flow over a step is analyzed. This work helps to explain some of the differences between the measurements by Catlett (2010) in a companion study at Virginia Tech and the LES based predictions presented by Ji and Wang(2010). The previous studies of the problem had used a low frequency approximation for the Greens function. The work presented here shows that, at the frequencies and flow Mach numbers considered by Catlett(2010), the low frequency approximation leads to incorrect predictions of the far field sound. The

exact Greens function for a step is given in Part II of this report and the importance of the diffracted field is identified.

Part III of this report focuses on flat plate boundary layers and the flow downstream of a forward facing step as measured Dr. William Devenport in a companion study at Virginia Tech. The previous analyses used the inviscid form of the linearized equations of motion to model the turbulent flow and in the last year the modeling has been improved to include viscous terms. In addition the non linear interactions are included as source terms for fully developed turbulence. The results have been compared to the experimental measurements reported by Awasthi et al (2011) and predictions are made of the velocity spectra and the surface pressure spectra.

## Table of Contents

# Part 1a:Turbulence Modeling for a Plane Wake

## 1.1 Introduction

In a recent study (Glegg *et al*(2010)), a method for calculating the surface pressure spectra below a turbulent boundary layer was developed which is based on the solution to the unsteady Euler equations and the Reynolds averaged Navier Stokes equations. It was shown that the unsteady velocity in a two dimensional linearized shear flow could be modeled using a distribution of vortex sheets. Each vortex sheet is convected at the local mean flow speed and its distribution can be used to specify all three components of the turbulent flow. The unsteady pressure, the two point velocity correlation functions, the turbulent kinetic energy and surface pressure wavenumber spectra was obtained directly from this equation in terms of the mean square value of the vortex sheet strength. Since RANS calculations give the distribution of turbulent kinetic energy in the flow, it was possible to invert the spatial distribution of turbulent kinetic energy to obtain the vortex sheet strength, and use the result to calculate all the statistical details of the unsteady flow. However, in this approach the specification of a turbulent energy spectrum that scales on the dissipation length scale was required and this is difficult to model universally.

In the first part of this study the approach described above was extended to turbulent flows in two dimensional wakes. Wake flows are more challenging than two dimensional boundary layers because the flow is continuously evolving in the downstream direction in a self similar manner. The theoretical approach was modified to allow for self similarity and the results were compared to experimental data of the two point velocity correlation functions in turbulent wakes (Devenport et al, 2001) with some success.

## 1.2 Theory for the turbulence of a wake flow

We will consider small velocity perturbations $(u,v,w)$ in a parallel shear flow defined, in cartesian coordinates $(x,y,z)$, by the mean velocity $U(y)$ in the $x$ direction (see figure 1). The linearized form of the Navier Stokes equations and the continuity equation can be used to obtain the Orr Sommerfeld equation for the upwash component of the velocity (see for example Hallbäck 1996)

(1)

$$\frac{D}{Dt}(\nabla^2 v) - \frac{\partial^2 U}{\partial y^2}\frac{\partial v}{\partial x} - \frac{1}{R_e}\nabla^4 v = 0$$

For a turbulent flow which is time stationary, but may not be homogeneous in the $x$ direction, we will consider the solution of this equation in the form

(2)

$$v = \sum_{n=1}^{\infty} a_n v^{(n)}(y) e^{-i\omega t + i\alpha_n x - i\beta z} \qquad \int_{-\infty}^{\infty} |v^{(n)}(y)|^2 \, dy = L(x)$$

where $\alpha_n$ are the eigenvalues of the solution and are assumed to be slowly varying in the flow direction, so the flow is at least locally homogeneous.

The other components of the velocity can be obtained by considering the vorticity in the $y$ direction given by

(3)

$$\eta = \frac{\partial u}{\partial z} - \frac{\partial w}{\partial x}$$

Combining this with the continuity equation (Hallbaek,1996) then gives the mode shapes for the other two velocity components as

(4)

$$u^{(n)} = \frac{-i}{\lambda_n^2}(\alpha_n \frac{\partial v^{(n)}}{\partial y} - \beta \eta^{(n)}) \qquad w^{(n)} = \frac{-i}{\lambda_n^2}(\beta \frac{\partial v^{(n)}}{\partial y} + \alpha_n \eta^{(n)})$$

where $\lambda_n^2 = \alpha_n^2 + \beta^2$. To bring the system to closure we use the vorticity equation for the $\eta$ component which gives

(5)

$$\frac{D\eta}{Dt} - \frac{1}{R_e}\nabla^2 \eta = -\frac{\partial U}{\partial y}\frac{\partial v}{\partial z}$$

and at high Reynolds number this gives

(6)

$$(-i\omega + U\frac{\partial}{\partial x})\eta - i\beta \frac{\partial U}{\partial y}\sum_{n=1}^{\infty} a_n v^{(n)}(y) e^{-i\omega t + \alpha_n x - i\beta z} = 0$$

The solution to this equation is then readily obtained by assuming that the vortiety is initially zero and gives the modes of the vortieity in terms of the upwash veloeity modes

(7)

$$\eta = \sum_{n=1}^{\infty} a_n \eta^{(n)}(y) e^{-i\omega t + i\alpha_n x - i\beta z}$$

$$\eta^{(n)}(y) = i\left(\frac{x}{U}\frac{\partial U}{\partial y}\right)\beta v^{(n)}(y)\tilde{\delta}_n(\omega, x, y) \qquad \tilde{\delta}_n(\omega, x, y) = \frac{\left(1 - e^{i(\omega/U - \alpha_n)x}\right)}{i(\alpha_n - \omega/U)x}$$

Hence equations (2), (4) and (7) form a closed set of equations which can be solved to obtain each component of the veloeity perturbations in terms of a single set of coeffieients $a_n$. The vorticity modes are dependent on $x$, but the $x$ dependenee is small for self similar flows (such as 2D wakes,axisymetrie wakes and mixing layers) whieh satisfy the eondition that

(8)

$$\frac{x}{U}\frac{\partial U}{\partial y} = \frac{W}{\Delta} f'(y/L)$$

where $W$ and $\Delta$ are constants and $L$ is the wake width.

The turbulent shear stresses ean be obtained by taking the expected valuc of the veloeity components and noting that if the mode amplitudes are uncorrelated then the veloeities are statistically stationary in time and locally homogeneous in the $x$ and $z$ directions. We also need to

intcgrate over all frequencies and spanwise wavenumbers to obtain the fluctuations at a point. Applying these steps leads to a description of the turbulent stress in the upwash direction as

(9)

$$\sigma_{vv}(y) = \int_{-\infty}^{\infty}\int_{-\infty}^{\infty}\sum_{n=1}^{\infty} A_n(\omega,\beta)V^{(n)}(y)d\omega d\beta \qquad V^{(n)}(y) = \mid v^{(n)}(y)\mid^2$$

similarly for the other two components of the flow we have,

(10)

$$\sigma_{uu} + \sigma_{ww} = \int_{-\infty}^{\infty}\int_{-\infty}^{\infty}\sum_{n=1}^{\infty} A_n(\omega,\beta)\left\{U^{(n)}(y) + \frac{\beta^2}{\lambda_n^2}\left(\frac{x}{U}\frac{\partial U}{\partial y}\right)^2 V^{(n)}(y)\tilde{\delta}^2(\omega,x,y)\right\}d\omega d\beta$$

$$U^{(n)}(y) = \mid \frac{\partial v^{(n)}(y)}{\partial(\lambda_n y)}\mid^2$$

the shear stress is then

(11)

$$\sigma_{uv} = -\left(\frac{x}{U}\frac{\partial U}{\partial y}\right)\int_{-\infty}^{\infty}\int_{-\infty}^{\infty}\sum_{n=1}^{\infty}\frac{\beta^2}{\lambda_n^2}A_n(\omega,\beta)V^{(n)}(y)\,\mathrm{Re}(\tilde{\delta}(\omega,x,y))d\omega d\beta$$

To a good approximation $\mathrm{Re}(\tilde{\delta}) = \mid \tilde{\delta}\mid^2$, so we can simplify (10) and specify the tke as

(12)

$$\kappa(y) \approx \frac{1}{2}\int_{-\infty}^{\infty}\int_{-\infty}^{\infty}\sum_{n=1}^{\infty} A_n(\omega,\beta)(U^{(n)}(y) + V^{(n)}(y))d\omega d\beta - \frac{1}{2}\left(\frac{x}{U}\frac{\partial U}{\partial y}\right)\sigma_{uv}$$

If we ean solve this equation for the unknown eoeffieients $A_n$ then we ean use the result to obtain eaeh of the stresses and the two point correlation of the veloeity fluetuations. For example the two point eorrelation of the upwash velocity is given as

(13)

$$R_{vv}(y,y') = \int_{-\infty}^{\infty}\int_{-\infty}^{\infty}\sum_{n=1}^{\infty} A_n(\omega,\beta)v^{(n)}(y)v^{(n)}(y')d\omega d\beta$$

The analysis given above deseribes how all the turbulent flow quantities of interest ean be speeified in terms of a single set of mode amplitudes $A_n$ . To bring the system to elosure it is neeessary to invert any one of the above equations to obtain the mode amplitudes. However the mode amplitudes are also dependent on the frequeney and the spanwise wavenumber and so it is also neeessary to assume so form for the energy distribution of the turbulenee.

### 1.3 Approximate Solution for the Continuous Modes

In many flows, espeeially the wake flow which is of interest here, we can make the approximations that the Reynolds number is very large and that $\lambda_n^2 U >> \partial^2 U / \partial y^2$ and so the last

two terms in equation (1) are small in comparison with the other terms giving the approximate equation

(14)

$$(\omega-\alpha_n U)(\frac{\partial^2 v^{(n)}}{\partial y^2}-\lambda_n^2 v^{(n)})\approx 0$$

The solution to this equation is obtained directly using

(15)

$$(\frac{\partial^2 v^{(n)}}{\partial y^2}-\lambda_n^2 v^{(n)})\approx q^{(n)} \qquad (\omega-\alpha_n U(y))q^{(n)}(y)=0$$

from which it follows that

(16)

$$q^{(n)}(y)=\mu\delta(y-y_n) \qquad v^{(n)}(y)=\int_{y_1}^{y_2} G(y\mid y')q^{(n)}(y')dy'=\mu G(y\mid y_n)$$

where $y_n$ is the solution to the equation $\omega=\alpha_n U(y_n)$ , $G(y/y_n)$ is the Greens function for Poissons equation which satisfies the boundary conditions of the flow, and $\mu$ is a scaling factor determined by (2) and is

(17)

$$\mu=\sqrt{\frac{L}{\int_{-\infty}^{\infty}|G(y\mid y_n)|^2\,dy}}$$

It is then relatively simple to complete the integrals needed in equations (9)-(13) using these modes and the approach given by Glegg *et al* 2009.

### 1.4 Determination of Mode Amplitudes

One of the important features of the turbulent velocity modes in the wake is that they can also be used to define the turbulent kinetic energy the wake, as given by equation (12). The turbulent kinetic energy is an output from RANS calculations and so, in principle, we can estimate $A_n$ if $U^{(n)}$ and $V^{(n)}$ are known. The approach used here is the solve the Orr Sommerfeld equations for the wake flow to obtain the modes, and use these as a basis for solving of the mode coefficients. However, some additional modeling is required to give the spectral content of the modes. To achieve this we assume that the coefficients $A_n(\omega,\beta)$ can be written as the product of a universal energy spectrum $E(\lambda L)$ and a mode amplitude in the form

(18)

$$A_n(\omega,\beta)=\tilde{A}_n E(\lambda_n L) \qquad \lambda_n=\sqrt{\alpha_n^2+\beta^2}$$

The universal energy spectrum is modeled by a von Karman energy spectrum (see Glegg et al (2008)) and is consistent with the energy cascade of turbulent scales. It depends on a lengthscale

$L$ which also has to be modeled or calculated from the dissipation in the RANS calculation (Glegg et al (2008)). If the turbulent kinetic energy is known at $y_m$ locations in the flow and the mode-shapes are determined by the solution to the Orr Sommerfeld equation then we can use a collocation scheme to determine the mode amplitudes by solving the equation

(19)

$$\kappa(y_m) = \sum_{n=1}^{M} \tilde{A}_n Q_{mn} \qquad Q_{mn} = \frac{1}{2} \int_{-\infty}^{\infty} \int_{-\infty}^{\infty} E(\lambda_n L) |\mathbf{u}^{(n)}(y_m, \omega, \beta)|^2 \, d\beta d\omega$$

Once these coefficients have been determined it is possible to predict all the two point statistics of the flow and the turbulent velocity spectra.

### 1.5 Numerical Verification of Results

This approach has been used to analyze the turbulent flow in a blade wake based on the measurements of Devenport et al (2001). These give the details of all three velocity components, their two point statistics and spectra as a function of $y$ and $x$ for the wake behind a NACA 0012 airfoil at zero angle of attack at a Reynolds number of $3.28 \times 10^5$ . The turbulent kinetic energy (tke) distributions are given at multiple locations downstream of the trailing edge and these are found to be self similar and to collapse onto a single line as shown in figure 2. Using the approach given above the mode amplitudes are obtained from the distribution of tke and are shown in figure 3. To verify that the approach is valid we have used these mode amplitudes to calculate the distributions of turbulent stresses $\sigma_{vv}$ and $\sigma_{uu}$, and the two point correlation function $R_{vv}(y,\Delta y)$ of the velocity in the $y$ direction at different reference locations $y$ across the wake. The results are shown in figures 4-6 and are successfully compared to experimental results. Figure 6 is a good test of the approach because the correlation function is not symmetric for reference locations that are displaced from the wake centerline.

In Figures 7 and 8 the estimated spectra of the $v$ and $u$ velocity components are given, and show reasonable agreement with the measurements.

### 1.6 Conclusions

In this study we have developed a method for extracting two point statistics from the distribution of turbulent kinetic energy in self similar flows. The approach is to develop a modal description of the turbulent velocity fluctuations based on the solution to the Orr Sommerfeld equation and use this to model the distribution of turbulent kinetic energy within the flow in terms of a set of unkown coefficients. If the distribution of the tke is available, either from measurements or RANS calculations, then the model can be inverted to obtain the unknown coefficients.

This approach has been applied to the flow in a turbulent wake based on the measurements of Devenport *et al* 2001 with very encouraging results. The model has successfully predicted the turbulent stresses and the two point correlation function of the upwash velocity fluctuations.

## Part 1b:Turbulence Modeling for Rotor Stator Interaction Noise

### 1.7 Introduction

Turbomachinery broadband noise is often dominated by the turbulence in the rotor wakes interacting with downstream stator vanes. The accepted approach for analyzing this problem is to model the turbulence incident on the stator vanes by a locally homogeneous turbulent flow whose spectrum can be defined by a von Karman or Liepmann model, with a specified turbulence intensity and length scale. This is a very simplistic model of the complex turbulent flow downstream of a rotor, which is dominated by rotating wake flows, secondary flows and end wall effects. In an earlier paper Glegg and Devenport (2001(b)) proposed a more general approach to turbulence modeling in complex flows based on proper orthogonal decomposition of the unsteady flow incident on the stator. The limitation of this approach was the determination of the proper orthogonal modes. In this paper we will revisit this problem and show how the modes of the flow can be obtained from the solutions to the linearized Navier Stokes equations, or in the case of quasi two dimensional flows, the Orr Sommerfeld equations. We will illustrate the procedure by showing results for a simple idealized model of an oblique blade wake interaction.

### 1.8 Sound Radiation from an Oblique Blade Wake Interaction

An oblique blade wake interaction occurs when the wake from an upstream blade is cut by a downstream blade at an angle, as is typical of a rotor wake stator blade interaction. The wake is modeled with a two dimensional mean flow profile which does not vary along the wake axis, and the cutting angle is defined as the angle between the spanwise coordinate of the blade and the axis of the wake (see Figure 1). The wake coordinates are specified as $(x,y,z)$ and the mean flow velocity in the wake is $U(y)$ in the direction of the $x$ coordinate. The blade is defined in terms of coordinates $(x_b,y_b,z_b)$ where $x_b$ is the chordwise direction and $y_b$ is the spanwise direction. The acoustic field from the blade wake interaction can be calculated from the unsteady loading on the blade surface, which, in ducted fan applications, can be coupled with the duct modes using the approach given by Glegg and Walker (1999). Here we will simplify the problem by considering the radiation from the blade in the absence of the duct. This gives an idealization of a rotor wake stator interaction which is suitable for identifying the principle features of turbulent wake flow that cause broadband fan noise from rotor stator interactions, without the complexity introduced by the blade response function for a high solidity stator in a duct.

Amiet (1974) gives the solution to the general problem of an unsteady flow incident on a blade in a uniform mean flow. The acoustic field is defined in terms of the unsteady loading on the blade surface, which is determined by the blade response to a harmonic gust. If the incoming gust has an upwash component on $z_b=0$ of the form

$$w_o e^{-i\omega t+i\gamma_o x_b+i\nu y_b}$$

then Amiet's blade response function gives the unsteady loading on the blade as

$$F(x_b, y_b, t) = w_o g(x_b, \gamma_o, v) e^{-i\omega t + i v y_b}$$

For the oblique blade wake interaction problem we will model the unsteady flow in the wake by the solution to the Orr Sommerfeld equation for the unsteady flow in the wake. This gives a modal solution for the unsteady flow in the wake, which is of the form

$$\mathbf{u}(x,y,z,t) = \sum_{n=1}^{\infty} \int_{-\infty}^{\infty} \int_{-\infty}^{\infty} a_n(\omega,\beta)\mathbf{u}^{(n)}(y,\omega,\beta) e^{-i\omega t + i\alpha_n(x)x + i\beta z} d\beta d\omega$$

where $\alpha_n(x)$ are the eigenvalues of the solution and can be assumed to be slowly varying in $x$, and $\mathbf{u}^{(n)}$ are the eigenvectors or modes of the solution. This expansion of the velocity has some important features that follow from the statistical nature of the turbulent flow. We can assume that the turbulent velocity fluctuations are stationary in time and homogeneous in the $z$ direction. Within the limit that $\alpha_n(x)$ is slowly varying we can also assume that the turbulent velocity fluctuations are homogeneous in the direction of the flow. It follows that the coefficients $a_n(\omega,\beta)$ are uncorrelated for different values of $n,\omega$ and $\beta$ and consequently, that the uncorrelated modes for the wake flow are

$$\mathbf{u}^{(n)}(y) e^{-i\omega t + i\alpha_n(x)x + i\beta z}$$

We can then proceed to analyze the oblique blade wake interaction problem in exactly the same way as was done by Glegg and Devenport (2001(a)), defining the upwash from the mode velocity and the cutting angle of the wake, and calculating the unsteady load and the acoustic radiation for each mode independently to give the acoustic pressure at an observer located at $\mathbf{x}$ as $p^{(n)}(\mathbf{x},\omega)$. Since each mode is uncorrelated the spectral density of the acoustic pressure is

$$S_{pp}(\mathbf{x},\omega) = \sum_{n=1}^{\infty} \int_{-\infty}^{\infty} A_n(\omega,\beta) |\, p^{(n)}(\mathbf{x},\omega)|^2 \, d\beta \qquad A_n(\omega,\beta) = \frac{\pi}{T} Ex[|\, a_n(\omega,\beta)|^2]$$

The important feature of this result is that the acoustic field for each mode can be readily calculated, and the characteristics of the acoustic field can be related to the features of each mode, but it remains to determine the mode amplitudes.

### 1.9 Acoustic Predictions

Using the results of Part 1(a) it is possible to carry out acoustic predictions for the sound radiation from a blade wake interaction at different cutting angles. In figure 9 we show some preliminary results of the effect of cutting angle on the far field noise. We note that as the cutting angle is reduced the radiated sound level is increased significantly. This is caused by two different effects. First, at smaller cutting angles the wetted surface area of the blade wake interaction is larger, and secondly the upwash is impacted by different components of the turbulent velocity as the cutting angle is changed. For a perpendicular blade wake interaction (90 deg cutting angle) the upwash on the blade is determined by the $z$ component of the turbulence in the wake. For a 45 deg cutting angle the upwash is determined equally by the $z$ and the $y$ component of the upwash. To accurately assess the importance of the cutting angle on the

radiated noise it is necessary to determine the relative amplitude and wavenumber spectra of these two different velocity components. The modeling approach described here allows this to be done by utilizing the solution to the Orr Sommerfeld equation for the unsteady flow in the wake. This is a far more robust approach than one that assumes a homogeneous turbulent flow model.

### 1.10 Conclusions

This paper describes a new approach for describing inflow turbulence for leading edge noise problems. The unsteady inflow is modeled by the Navier Stokes equations linearized relative to the mean flow velocity. The resulting solutions give the relative magnitudes of all velocity components throughout the flow, and this provides a model of the local tke in the flow that can be matched to the tke calculated by RANS models. The resulting unsteady flow model can then be used to carry out acoustic predictions of leading edge noise. This approach has been shown to successful match measurements of two point correlations and spectra of the turbulent flow in the wake of a NACA 0012 airfoil, and the application to leading edge noise has been demonstrated. The extension of this method to ducted flows and the wake of a rotor is also possible based on the model of the linearized flow in a circular duct given by Atassi (2005).

### References


Amiet, R. K., "Acoustic Radiation from an Airfoil in a Turbulent Stream," Journal of Sound and Vibration, Vol. 41, No. 4, 1975, pp. 407–420.

Atassi, O. V. Propagation and Stability of Vorticity-Entropy Waves in a Non-Uniform Flow, Journal of Fluid Mechanics, Vol. 575, pp. 149-176

Devenport W J, Muthanna C and Glegg S A L, 2001, "Two-Point Descriptions of Wake Turbulence with Application to Noise Prediction", AIAA Journal, vol. 39, no. 12, pp. 2302-2307

S.A.L. Glegg and N.Walker, CEAS/AIAA paper 99-1888, "Fan Noise From Blades Moving Through Boundary Layer Turbulence", Fifth Joint CEAS/AIAA Aeroacoustics Conference, Seattle, WA, May 1999.

Stewart A.L. Glegg and William J. Devenport, "Proper Orthogonal Decomposition Of Turbulent Flows For Aeroacoustic and Hydroacoustic Applications", Journal of Sound and Vibration, Vol. 239(4), pp767-784, 2001(a)

S.A.L. Glegg, and W J Devenport, CEAS/AIAA paper 2001-2242, "Rotor stator interaction noise from blade wakes", Seventh Joint AIAA/CEAS Aeroacoustics Conference, Maastrict, The Netherlands, May 2001(b).

S.Glegg, B.Morin, O. Atassi, and R.Reba "Using RANS calculations to provide predictions of trailing edge noise" AIAA Paper 2008-2993, presented at the 14th AIAA/CEAS Aeroacoustics Conference, Vancouver, May 2008

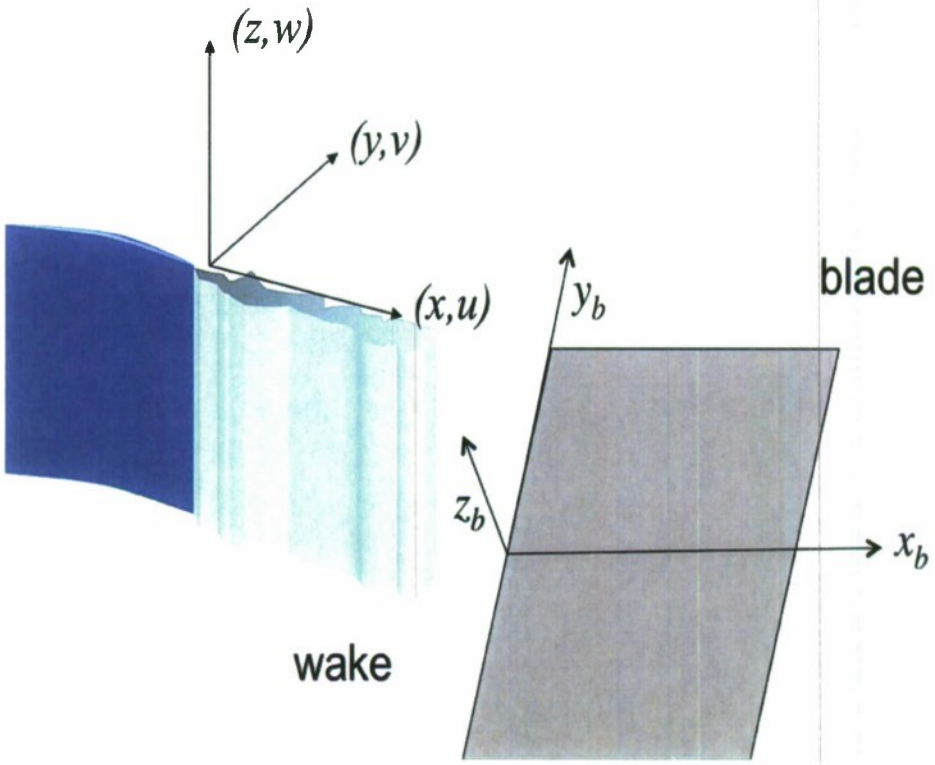


Figure 1: the coordinate system for a simple wake incident on an isolated blade

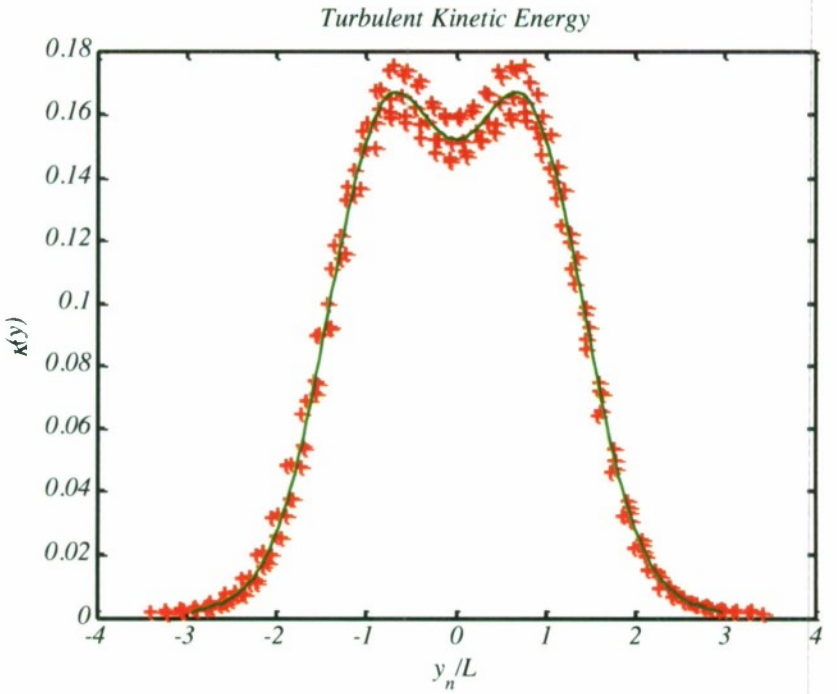


Figure 2: The collapse of the tke in a turbulent wake behind a NACA 0012 airfoil as a function of displacement from the centerline. The data is self similar an collapses on the wake half width $L$. The mean line is the data fit obtained from the modal solution.

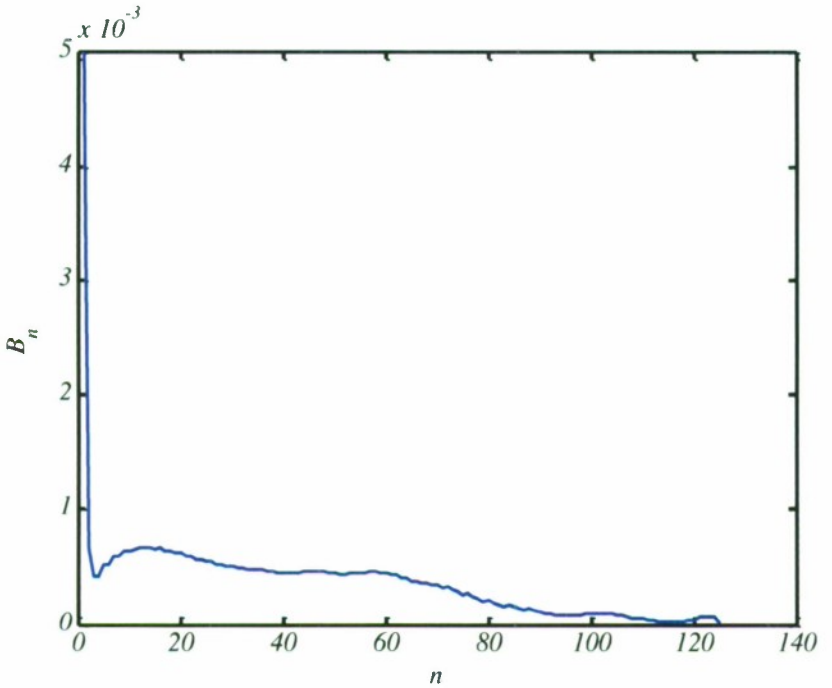


Figure 3: The mode amplitudes calculated from the distribution of kinetic energy

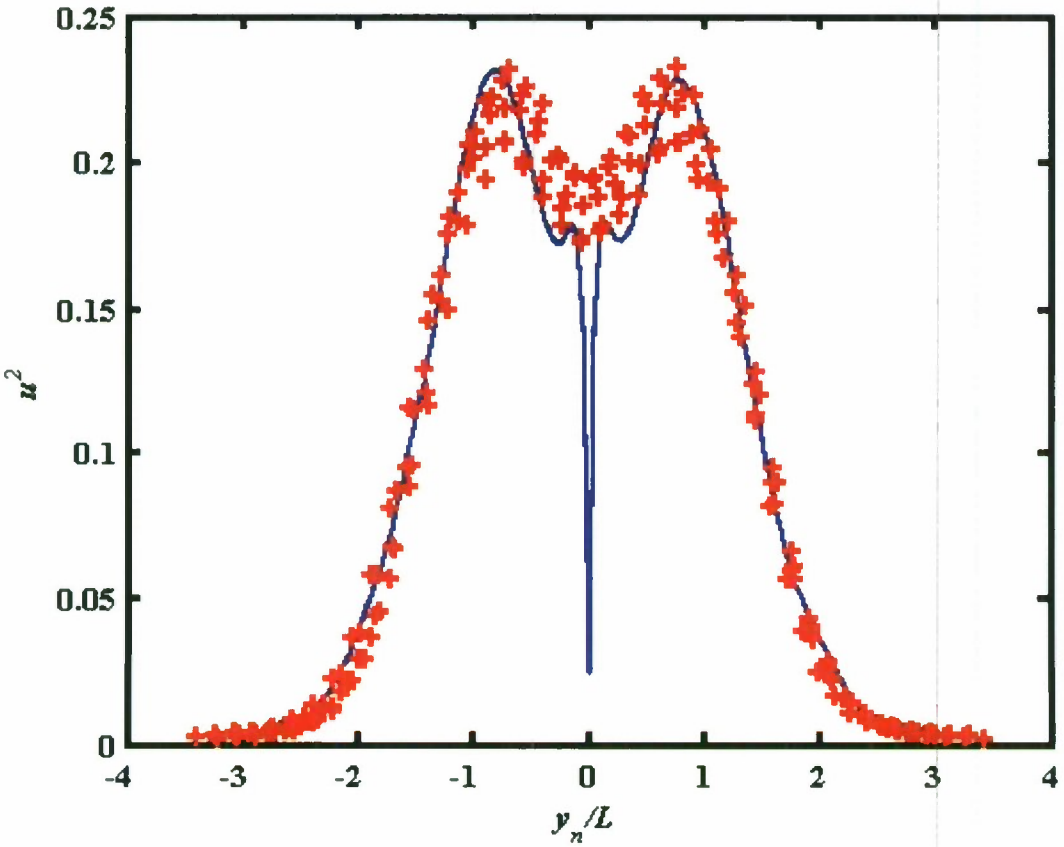


Figure 4: The estimated distribution of $u^2$ across the wake.

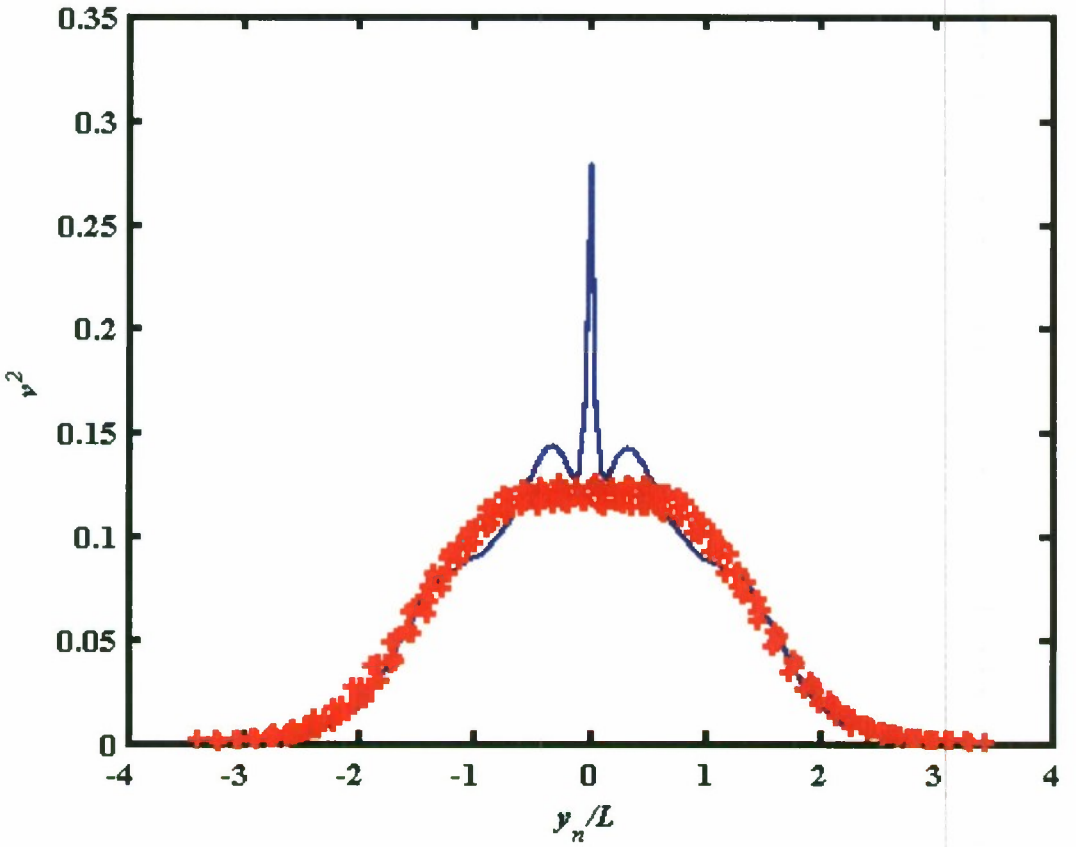


Figure 5: The estimated distribution of $v^2$ across the wake.

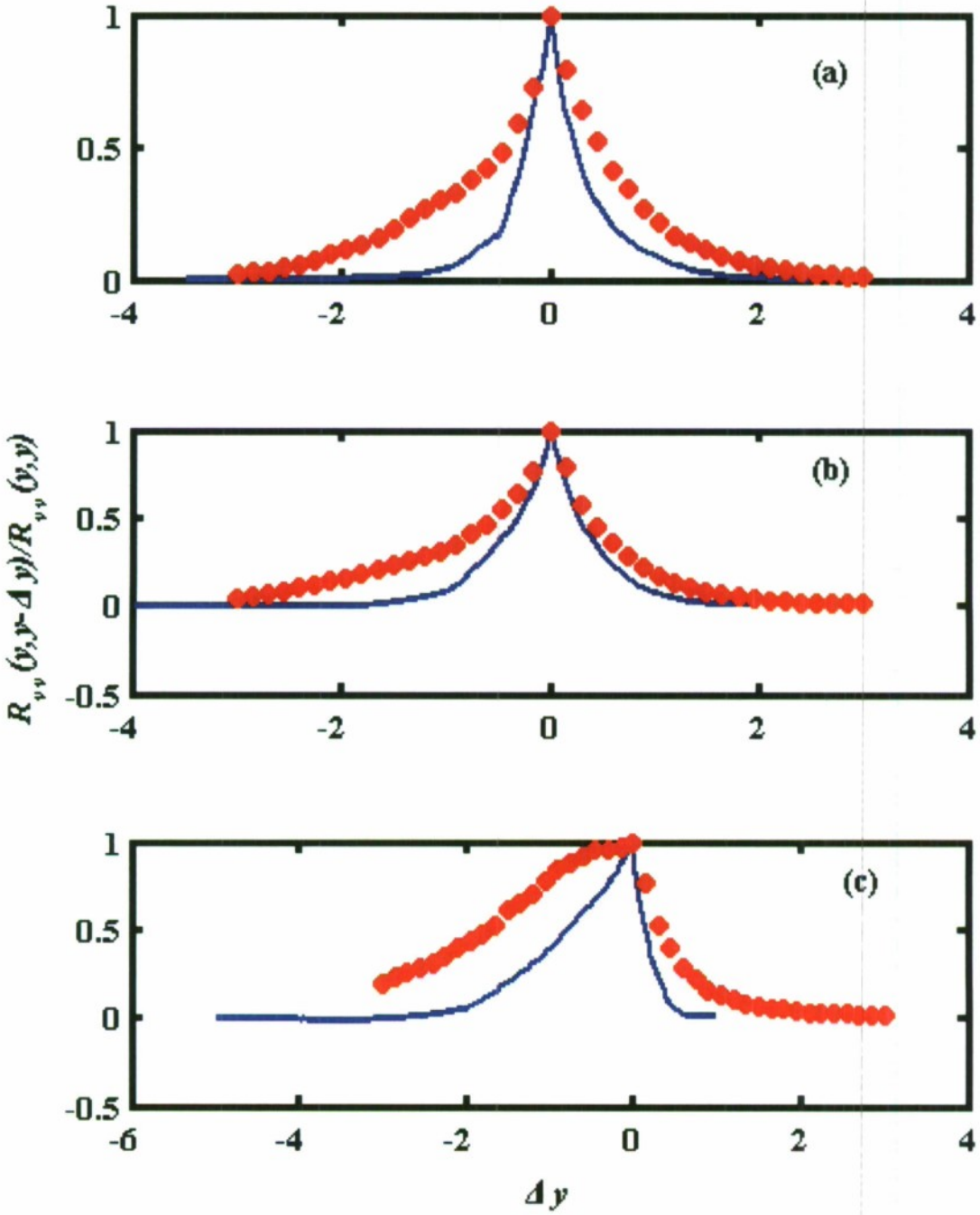


Figure 6: The two point correlation function $R_w(y,\Delta y)$ for different reference locations $y$ across the wake (a) $y=0.5L$, (b) $y=L$ (c) $y=2L$

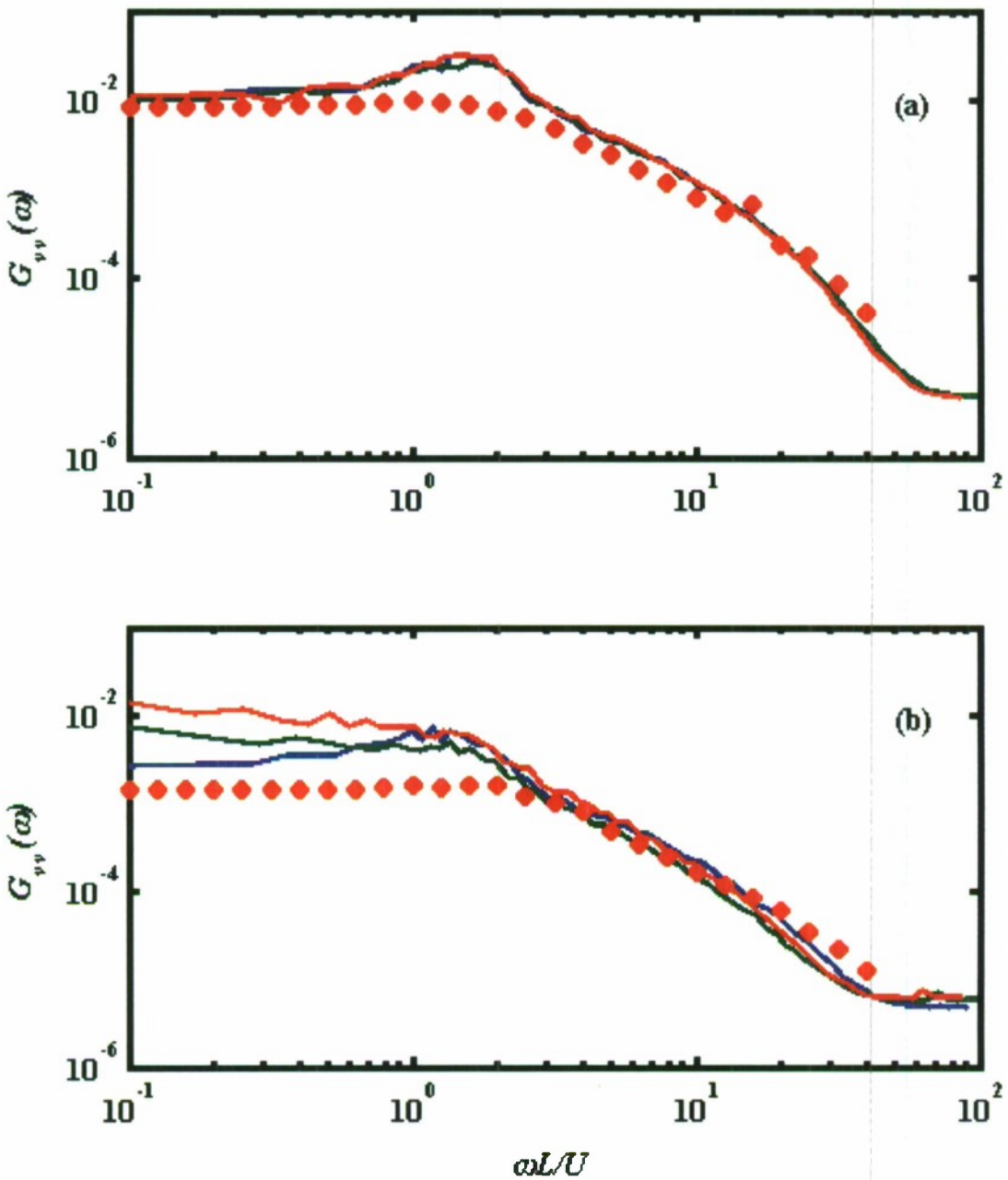


Figure 7: The speetra $G_{vv}$ at two different locations aeross the wake, (a) $y=L$ (b) $y=2L$

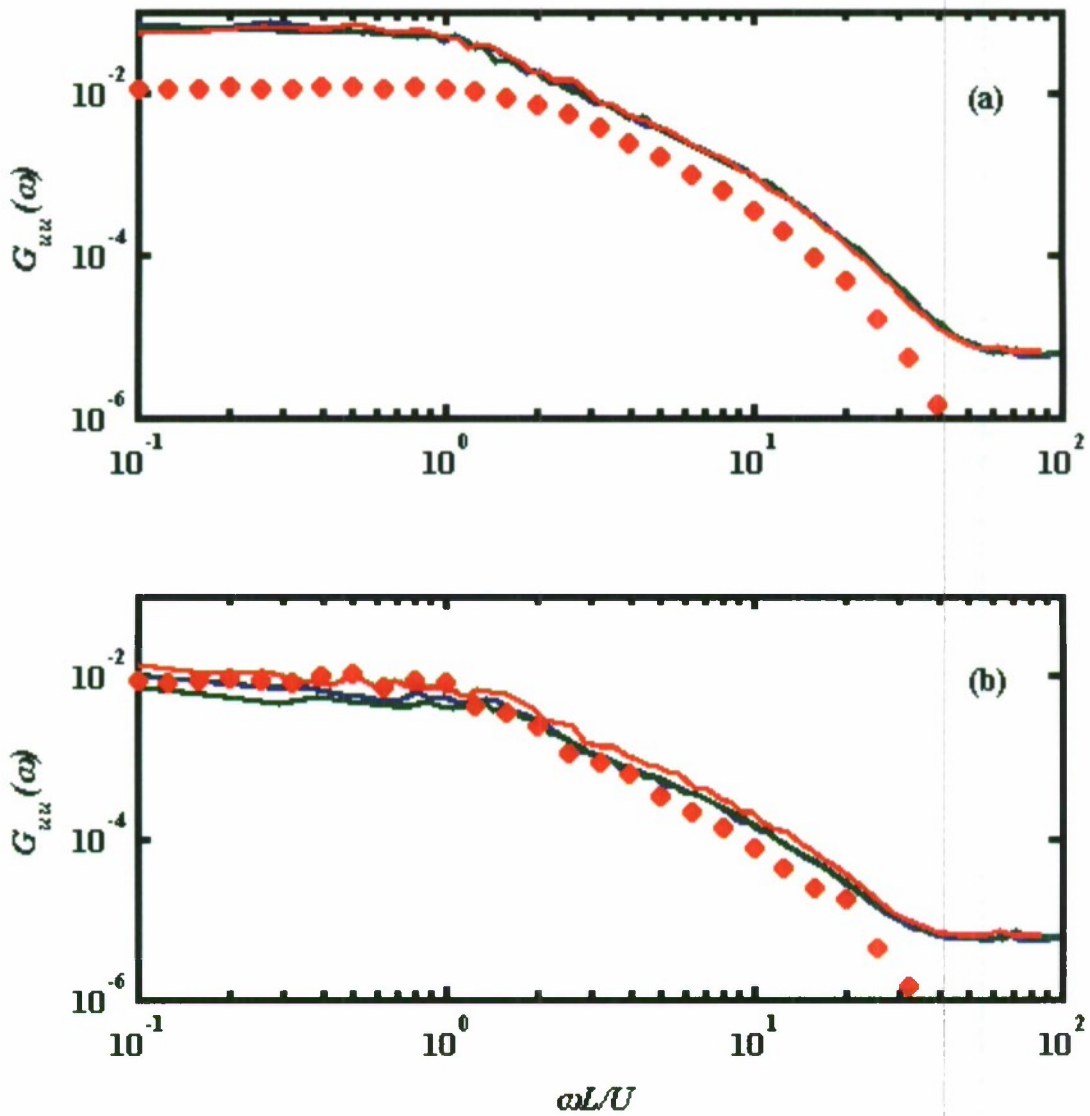


Figure 8: The spectra $G_{uu}$ at two different locations across the wake, (a) $y=L$ (b) $y=2L$

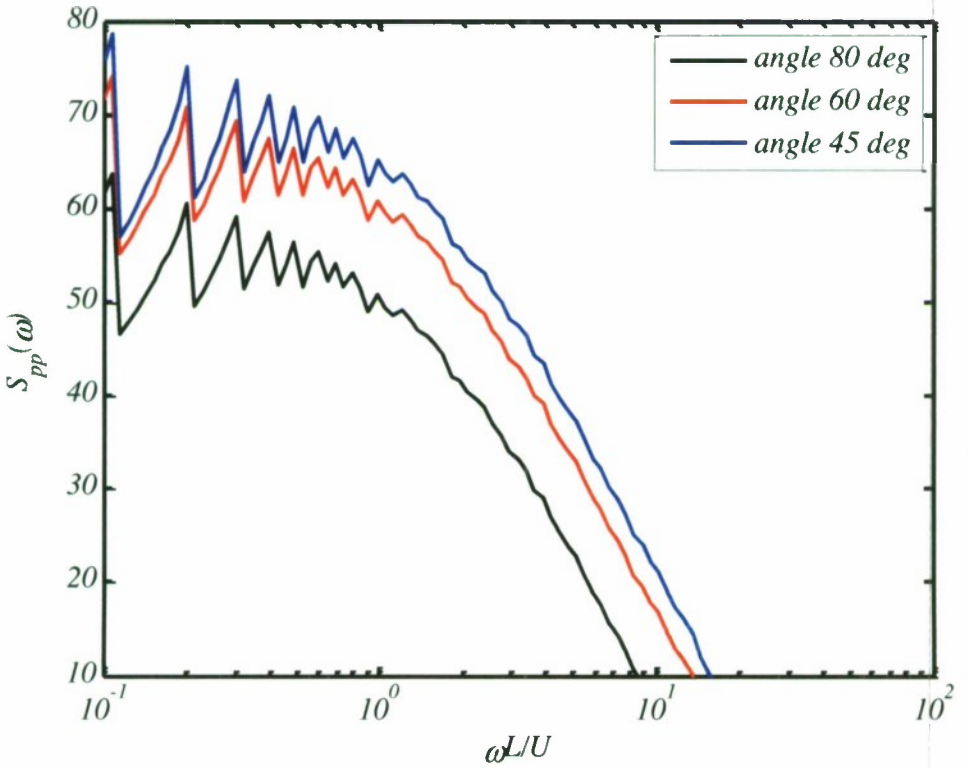


Figure 9: Predicted acoustic spectra for leading edge noise from an oblique blade wake interaction. $S_{pp}$ is given in dB with an arbitrary reference. Flow Mach number is 0.5.

## Part 2: The Tailored Greens Function for a Step

### 2.1 Introduction

In a recent article Ji and Wang(2010) described detailed Large Eddy Simulations (LES) of boundary layer flows over forward and backward facing steps. One of the objectives of this study was the calculation of the sound radiated by the interaction of the flow with the step. To carry out their calculations Ji and Wang made use of Howe's(1989) low frequency approximation for the Greens function tailored to the step geometry. This Greens function gives a far field directionality that is equivalent to a streamwise dipole and predicts there will be a null in the acoustic far field for an observer directly above the step. In contrast experimental measurements (Farabee and Zoccola(1998), Catlett(2010)) indicate that this is not the case and the directionality of the sound is relatively weak at low frequencies. Catlett(2010) also observed that there was an interference effect in the spectrum at high frequencies that could not be predicted by the low frequency approximation. In this paper the far field approximation for the Greens function tailored to the step geometry will be derived by applying the Weiner Hopf method. The result shows that the sound in the acoustic far field is only equivalent to a dipole at very low frequencies, and it has very different characteristics at higher frequencies. The far field sound spectrum can also be estimated and it is shown that the interference effect observed by Catlett(2010) is correctly indentified.

### 2.2 The Greens Function

The geometry for a step of height $b$ is shown in Figure 1 in terms of the Cartesian coordinates $(y_1,y_2,y_3)$. The origin of the coordinate system is at the bottom of the step and the surface is defined by $y_2=0$, $y_1>0$ and $y_2=b, y_1<0$. To calculate the far field Greens function we will use the adjoint method, which utilizes the principle of reciprocity. In this approach the source is placed at a location in the acoustic far field and the observer is placed in the vicinity of the step. The advantage of using this method is that the adjoint Greens function can be obtained by calculating the field scattered by the step due to sound from the far field source, and, local to the step, the incident field is well approximated by a plane wave. The Greens function for the source close to the step and the far field observer is then simply the adjoint Greens function with the source and observer positions reversed.

In the adjoint problem the source is placed at $x_i$ and the incident wave is given by $\exp(ikr-ikx_iy_i)/4\pi r$ where $r=|\mathbf{x}|$ is the distance of the source from the bottom of the step and $k$ is the acoustic wavenumber at the frequency $\omega$. The adjoint Greens function which satisfies the non penetration boundary conditions on $y_2=0$ is then given by

$$G_o(y_i \mid x_i) = \frac{e^{ikr-ikx_3y_3/r-ikx_1y_1/r}}{2\pi r}\cos(kx_2y_2/r) \qquad r>>|\mathbf{y}| \tag{1}$$

To satisfy the boundary conditions on the step we need to add solutions that correct for the non penetration boundary condition on the surfaces $y_2=b, y_1<0$ and $0<y_2<b$, $y_1=0$. We will treat these as the sum of two separate corrections $G_1$ and $G_2$. First we define $G_1$ as the solution that corrects $G_o$ to match the boundary conditions on the upper surface of the step, so it has the boundary conditions (see figure 2)

(2)

$$\left[\frac{\partial G_1}{\partial y_2}\right]_{y_2=0}=0 \qquad \left[\frac{\partial G_o}{\partial y_2}+\frac{\partial G_1}{\partial y_2}\right]_{y_2=b,y_1<0}=0$$

Secondly we define $G_2$ as the solution that corrects $G_o+G_1$ to match the boundary conditions on the face of the step, so it has the boundary conditions (see figure 3)

(3)

$$\left[\frac{\partial G_2}{\partial y_2}\right]_{y_2=0}=0 \qquad \left[\frac{\partial G_2}{\partial y_2}\right]_{y_2=b,y_1<0}=0 \qquad \left[\frac{\partial G_o}{\partial y_1}+\frac{\partial G_1}{\partial y_1}+\frac{\partial G_2}{\partial y_1}\right]_{0<y_2<b,y_1=0}=0$$

The solution for $G_1$ is obtained from the result given by Noble(1958) for the scattering of sound by a semi infinite two dimensional duct. If we represents the Greens function $G_o$ as the sum of two waves incident from the angles $\theta$ and $-\theta$, where $\cos\theta\cos\phi=x_1/r$, $\sin\theta\cos\phi=x_2/r$ and $\sin\phi=x_3/r$. Then we can write

(4)

$$G_o=A(e^{-ik_o y_1\cos\theta-ik_o y_2\sin\theta}+e^{-ik_o y_1\cos\theta+ik_o y_2\sin\theta}) \qquad A=\frac{e^{ik_o r-ikx_3y_3/r}}{4\pi r} \qquad k_o=k\sin\phi$$

and use the result given by Noble (1958) for scattering of plane waves by two semi infinite planes. The result is given by Noble's equation 3.25 as

(5)

$$G_1=\frac{A}{\pi}\int_{-\infty+i\tau}^{\infty+i\tau} S_-(\alpha)E(\gamma y_2)e^{-i\alpha y_1}d\alpha \qquad E(\gamma y_2)=\begin{cases}-\cosh(\gamma y_2)e^{-\gamma b} & 0<y_2<b\\ \sinh(\gamma b)e^{-\gamma y_2} & b<y_2\end{cases}$$

and

(6)

$$S_-(\alpha)=\frac{i\sin\theta\sin(k_o b\sin\theta)}{b(1+\cos\theta)L_+(k_o\cos\theta)L_-(\alpha)(\alpha-k_o)(\alpha-k_o\cos\theta)}$$

(7)

$$L_+(\alpha)L_-(\alpha)=\frac{\sinh(\gamma b)e^{-\gamma b}}{\gamma b} \qquad \gamma=(\alpha-k_o)^{1/2}(\alpha+k_o)^{1/2}$$

The choice of branch cut for the square roots is important and we choose the branches where $\mathrm{Re}((\alpha\pm k_o)^{1/2})>0$. The subscripts $\pm$ represent functions which are analytic for $\mathrm{Im}(\alpha)$ greater than or less than zero respectively, and specifics of $L_+$ and $L_-$ will be discussed later.

The next step is to determine the second correction which ensures the velocity on the step face is zero. We note that the sum of $G_o$ and $G_1$ result in waves which propagate from right to left along the duct defined by $0<y_2<b$, $y_1<0$ ( see Figure 3). To cancel the velocity at $y_1=0$ we introduce a wave which propagates from left to right along the duct so that the boundary condition is satisfied. The new wave will also be transmitted across the duct termination and propagate out of the duct and so will affect the region of interest. This problem is also discussed by Noble and for a wave $B_n\cos(n\pi(y_2-b)/b)\exp(i\kappa_n y_1)$, (where $\kappa_n=(k_0^2-(n\pi/b)^2)^{1/2}$, and has a positive imaginary part) propagating along the duct. The acoustic field is given by Noble equation (3.34) as

(8)

$$G_2 =$$

$$\sum_{n=0}^{\infty} B_n \left( \begin{array}{l} \cos(n\pi(y_2 - b)/b) e^{i\kappa_n y_1} \\ + \dfrac{ib}{2\pi}(k_o + \kappa_n) L_-(-\kappa_n) \displaystyle\int_{-\infty+i\tau}^{\infty+i\tau} \dfrac{(\alpha + k_o) L_+(\alpha) \cosh(\gamma y_2)}{\gamma(\alpha + \kappa_n)\sinh(\gamma b)} e^{-i\alpha y_1} d\alpha \end{array} \right) \qquad 0 < y_2 < b$$

and

(9)

$$G_2 = \sum_{n=0}^{\infty} B_n \left( -\frac{ib}{2\pi}(k_o + \kappa_n) L_-(-\kappa_n) \int_{-\infty+i\tau}^{\infty+i\tau} \frac{(\alpha + k_o) L_+(\alpha) e^{\gamma b}}{\gamma(\alpha + \kappa_n)} e^{-i\alpha y_1 - \gamma y_2} d\alpha \right) \qquad y_2 > b$$

To obtain the unknown coefficients $B_n$ we evaluate the field in the dueted region. Noble shows that by evaluating equation (4) we have

(10)

$$\left[G_o + G_1\right]_{0<y_2<b, y_1<0} = \sum_{m=0}^{\infty} C_m \cos(m\pi(y_2 - b)/b) e^{-i\kappa_m y_1}$$

where $C_m$ represents the residue at the poles of the integrand of (5) which lie in the upper half of the complex plane and are given in the appendix. Similarly we can evaluate (8) in the dueted region. The solution includes the waves propagating from left to right and the waves which are reflected from the duct termination at $y_1=0$, and can be expressed as

(11)

$$\left[G_2\right]_{0<y_2<b, y_1<0} = \sum_{m=0}^{\infty} \sum_{n=0}^{\infty} B_n \left(\delta_{mn} e^{i\kappa_m y_1} + R_{mn} e^{-i\kappa_m y_1}\right) \cos(m\pi(y_2 - b)/b)$$

where the reflection coefficients $R_{mn}$ are also given in the appendix. Using (10) and (11) in the last of the boundary conditions (3) and equating terms gives

(12)

$$\sum_{n=0}^{\infty} B_n(\delta_{mn} - R_{mn}) = C_m$$

If this series is truncated to a finite number of terms then this equation can be solved for the coefficients $B_n$, giving the complete solution for $G_2$.

### 2.3 Approximate Solutions

At very low frequencies we can show that $L_+(k_0) \sim 1$ and $B_o \sim C_o/2 = A$ and. Also the series expansion for $G_2$ is dominated by the $n=0$ term and so for $y_2 > b$ we can approximate

(13)

$$G_2 = \frac{-iAk_o b}{\pi} \int_{-\infty+i\tau}^{\infty+i\tau} \frac{L_+(\alpha)}{\gamma} e^{-i\alpha y_1 - \gamma(y_2 - b)} d\alpha$$

Applying the same approximations to $G_1$ in the region $y_2 > b$ , and utilizing equation (7) gives

(14)

$$G_1 = \frac{iAk_o b(1-\cos\theta)}{\pi} \int_{-\infty+i\tau}^{\infty+i\tau} \frac{\gamma L_+(\alpha)}{(\alpha-k_o)(\alpha-k_o\cos\theta)} e^{-i\alpha y_1-\gamma(y_2-b)} d\alpha$$

At moderate frequencies where $k_o b=1$ the situation is quite different. In this case we find from numerical evaluation that $B_o \sim C_o$ and that $B_n << B_o$, but we can not approximate the other terms. Then, for $y_2>b$ we obtain

(15)

$$G_2 = \frac{-2iA\sin(k_o b\sin\theta)L_-(-k_o)}{\pi\sin\theta L_+(k_o\cos\theta)L_-(k_o)} \int_{-\infty+i\tau}^{\infty+i\tau} \frac{L_+(\alpha)}{\gamma} e^{-i\alpha y_1-\gamma(y_2-b)} d\alpha$$

and

(16)

$$G_1 = \frac{iA\sin\theta\sin(k_o b\sin\theta)}{\pi(1+\cos\theta)L_+(k_o\cos\theta)} \int_{-\infty+i\tau}^{\infty+i\tau} \frac{\gamma L_+(\alpha)}{(\alpha-k_o)(\alpha-k_o\cos\theta)} e^{-i\alpha y_1-\gamma(y_2-b)} d\alpha$$

and we note that the scaling on $k_o$ and directionality associated with these functions is quite different from the low frequency approximation.

**2.5 Discussion**

The sound radiation from turbulent flow near rigid surfaces can be evaluated by using Lighthills acoustic analogy. The sound sources are specified by Lighthills stress tensor and the acoustic field is given by (Goldstein (1976))

(17)

$$\rho' c_o^2(x_i,\omega) = \int_V T_{ij}(y_i,\omega)\frac{\partial^2 G}{\partial y_i \partial y_j} dV$$

where $G$ is a tailored Greens function that satisfies the non penetration boundary condition on all the surfaces. The radiation efficiency of the sound sources is therefore given by $\partial^2 G/\partial y_i \partial y_j$ ,which, for flow over a step is given by the Greens function defined above. If we evaluate $\partial^2 G_o/\partial y_i \partial y_j$ it is found that the acoustic radiation scales as $k^2$ and this leads to a source of quadrupole order. In contrast if we evaluate $\partial^2 G_1/\partial y_1^2$ we find that this simple scaling is not present. If we model the Lighthills stress tensor for a turbulent eddy convected in the $y_1$ direction as

(18)

$$T_{ij}(y_i,\omega) = \tilde{T}_{ij} e^{i\omega y_1/U}\delta(y_2-h)\ell$$

where $h>b$ then, and $\ell$ is a length scale, then using the low frequency approximations we obtain

(19)

$$\rho' c_o^2(x_i,\omega) \approx \left(\frac{-2iAk_o bL_+(\omega/U)\ell}{\gamma_o}\right)\left(-(\omega/U)^2\tilde{T}_{11} - i(\omega/U)\gamma_o\tilde{T}_{12} + \gamma_o^2\tilde{T}_{22}\right)$$
$$\times\left(1-\frac{(1-\cos\theta)(\omega/U+k_o)}{(\omega/U-k_o\cos\theta)}\right)e^{-\gamma_o(h-b)}$$

where

(21)

$$\gamma_o = \sqrt{(\omega/U)^2 - k_o^2}$$

At very low Maeh numbers where $\omega/U >> k_o$ we ean approximate $\gamma_o \sim \omega/U$ and it follows that

(22)

$$\rho' c_o^2(x_i,\omega) \approx \left(-2iAk_o b\cos\theta\right)(\omega\ell/U)L_+(\omega/U)\left(-\tilde{T}_{11} - i\tilde{T}_{12} + \tilde{T}_{22}\right)$$

First we note that this result has the eharaeteristies of a streamwise dipole, sealing with $k_o$ and having a direetionality of $\cos\theta$. The sealing on flow speed ean be obtained by noting that $T_{ij}$ seales as $\rho U^2$ and $k_o$ scales as $M\omega/U$ where $M=U/c_o$, and $c_o$ is the speed of sound. Then at eonstant Strouhal number $(\omega b/U)$ the acoustic pressure seales as $U^3$ and the acoustic power output seales as $U^6$.

For the higher frequeneies the sealing is quite different. Equations (15) and (16) show that the sealing on frequcncy depends on $\sin(k_o b\sin\theta)$ and $L_+(k_o\cos\theta)$, so the field no longer has the eharaeteristies of a dipole.

The complete eharaeteristies of the direetionality of the sound generated by flow over a step can be ealeulated directly from

(23)

$$\rho' c_o^2(x_i,\omega) =$$
$$\left\{\frac{2iA\sin\theta\sin(k_o b\sin\theta)(\omega/U+k_o)}{(1+\cos\theta)L_+(k_o\cos\theta)(\omega/U-k_o\cos\theta)} - i\sum_{n=0}^{\infty}\frac{B_n(\kappa_n+k_o)(\omega/U+k_o)bL_-(-\kappa_n)}{(\omega/U+\kappa_n)}\right\}$$
$$\times(\ell/\gamma_o)L_+(\omega/U)\left(-(\omega/U)^2\tilde{T}_{11} - i(\omega/U)\gamma_o\tilde{T}_{12} + \gamma_o^2\tilde{T}_{22}\right)e^{-\gamma_o(h-b)}$$

This result has been evaluated to show the direetionality of the sound field at different non dimensional frequencies $k_o b=0.01,0.1,1$. For a backward facing step in a low Mach number flow ($M=0.02$) are shown in figure 4. At low frequeneies the direetionality has a minimum at $\theta=90^o$ and is similar to a dipole orientated in the direction of the flow. At high frequeneies the direetionality is impacted by interference effeets and is almost omnidireetional. Similar results are shown for a forward faeing step in Figure 5, (obtained from equation (23) with $U$ replaeed by $-U$) and it is hard to distinguish the difference. Howevcr at higher Maeh numbers ($M=0.2$) the direetionality is different as shown in figures 6 and 7, and the effeet of flow direction is morc marked with nulls pointing towards the direction of the flow.

Figure 8 shows the frequency dependence of the field at three different obscrver angles for a forward facing step at a Mach number of 0.2. It is impotant to note the interference dip that occurs when $k_o b\cos\theta=\pi$ and the lack of collapse of the aeoustic efficieney onto a single eurve. This indieates that sealing of experimental data on a single frequency parameter could be unsueeessful.

In Figure 9 show the speetrum of the far field sound is shown assuming a souree speetrum whieh seales as $(k_o h)^{-17/3}$ for an 11 mm step and observer positions that eorrespond to those measured by Catlett(2010). An arbitrary scaling factor has been added to align the plots so this is not an absolute prediction. Howevcr hc spectra show the interferenee dip and resonances at frequencies above 10kHz which were observed experimentally by Catlett (2010) and there is some eonsisteney between the measured levels at different angles at low frequencies.

## 2.6 Conclusion

The results given above discuss the sound radiation from turbulent flow over a step. It is concluded that the sound radiation is a consequence of scattering mechanism that can be modeled from solutions presented by Noble for scattering by parallel semi infinite plates. At very low frequencies the far field sound has the characteristics of a streamwise dipole and the sound from turbulent flow in the vicinity of the step scales with the sixth power of the flow velocity. At higher frequencies the there interference effects become important and the spectrum exhibits an dip at angles where $k_o h \sin\theta = n\pi$. The directionality and spectral characteristics are similar to those measured experimentally by Catlett(2010).


## Acknowledgments

The authors would like to thank Dr. Meng Wang for stimulating discussions on this issue.


## References


Catlett, M.R., 2010, "Flow Induced Noise from Turbulent Flow over Steps and Gaps", Master's Thesis, AOE Department, Virginia Tech. Avail: http://scholar.lib.vt.edu/theses/available/etd-05172010-192806/ .

Farabee, T. M., and Zoccola, P. J., 1998, "Experimental Evaluation of Noise due to Flow over Surface Steps", 1998 ASME International Mechanical Engineering Congress and Exposition.

Goldstein M 1976, *Aeroacoustics* McGraw Hill NY

Howe, M.S., 1989, "Sound Produced by Turbulent Boundary Layer Flow Over a Finite Region of Wall Roughness, and Over a Forward Facing Step", Journal of Fluids and Structures, 3, pp. 83-96.


## Appendix

The coefficients $C_m$ are obtained from (5) as

$$C_o = \frac{2A\sin(k_o b\sin\theta)}{k_o b\sin\theta L_+(k_o\cos\theta)L_-(k_o)}$$

$$C_m = \frac{-2A\sin\theta\sin(k_o b\sin\theta)L_+(\kappa_m)(m\pi)^2}{\kappa_m b(1+\cos\theta)(\kappa_m - k_o\cos\theta)(\kappa_m - k_o)b^2 L_+(k_o\cos\theta)} \qquad m>0$$

Similarly we obtain for the reflection coefficient:

$$R_{mn} = \frac{-\varepsilon_m(\kappa_m + k_o)(\kappa_n + k_o)L_-(-\kappa_n)L_+(\kappa_m)}{\kappa_m(\kappa_m + \kappa_n)}$$

where $\varepsilon_m = 1$ for $m>0$ and $\varepsilon_o = 0.5$.

*The Split Function*

Following Noble p104 we can define the split function

$$L_+(\alpha)=\left(\prod_{n=1}^{\infty}\left\{((1-(k_o b/n\pi)^2)^{1/2}-i\alpha b/n\pi\right\}e^{i\alpha b/n\pi}\right)$$

$$\times\exp\left[-i\frac{\alpha b}{\pi}(1-C+\ln(2\pi/k_o b))+\alpha b/2-(\gamma b/\pi)\cos^{-1}(\alpha/k)\right]$$

and $L_-(\alpha)=L_+(-\alpha)$.

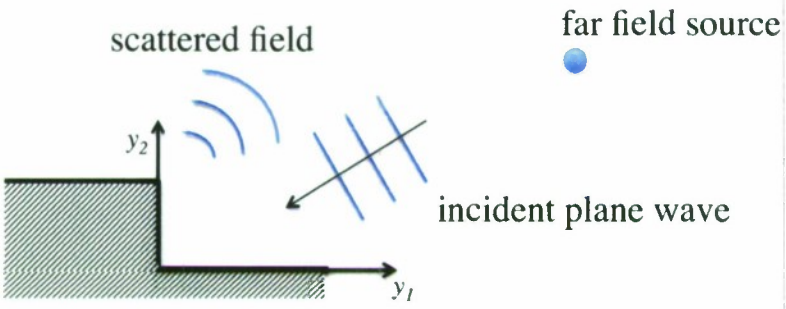


Figure 1: The coordinate system used to define the step and the adjoint problem

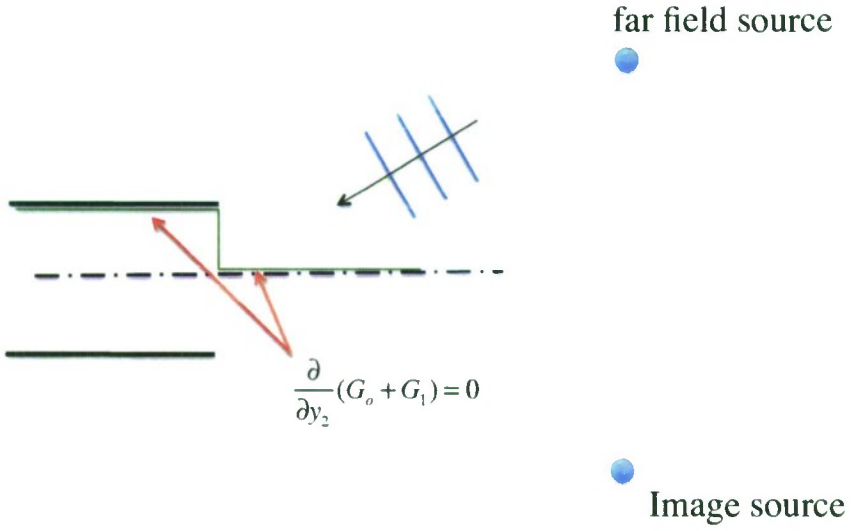


Figure 2: Schematic of the first decomposition which satisfies the boundary conditions on $y_2=b, y_1<0$ and $y_2=0, y_1>0$.

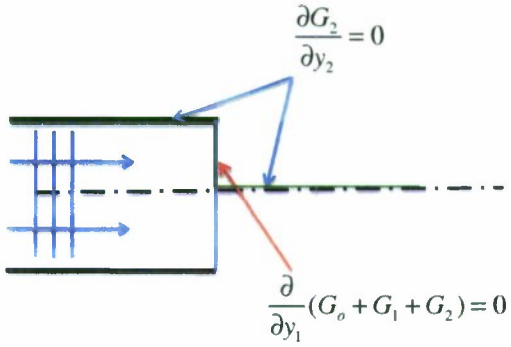


Figure 3: Schematic of the second problem that satisfies the boundary conditions on the face of the step.

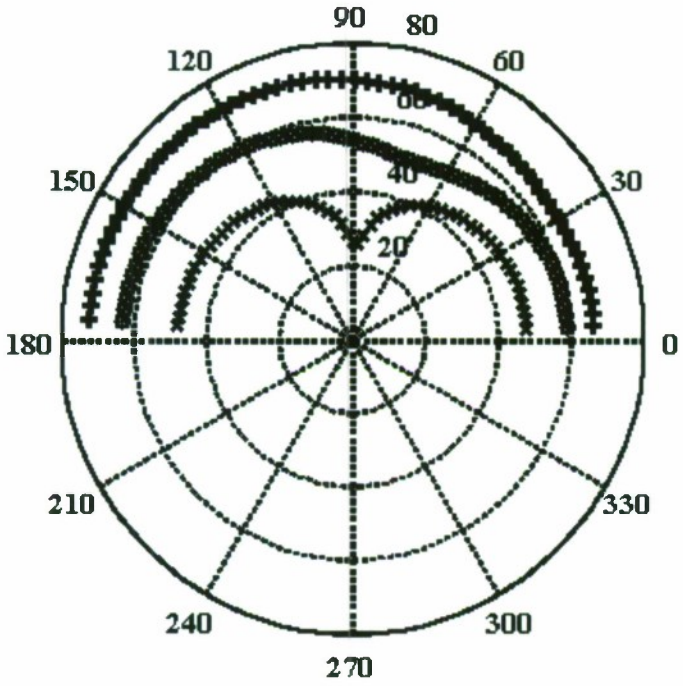


Figure 4: The Directionality of sound from sources near a backward facing step at a Mach number of 0.02. Levels are normalized by $k_o b$ and 50dB has been added to ensure positive values on all plots. –x-x- $k_o b=0.01$, -o-o-$k_o b=01$, -+-+- $k_o b=1$

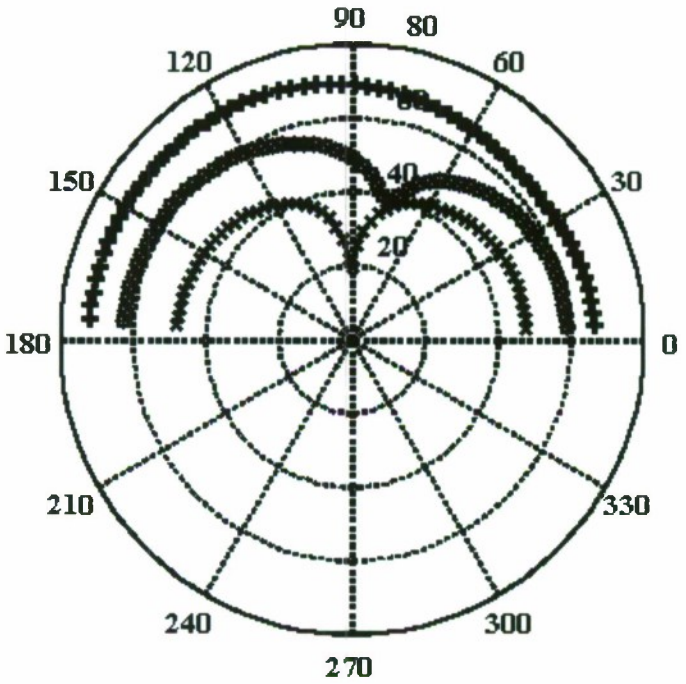


Figure 5: The Directionality of sound from sources near a forward facing step at a Mach number of 0.02. Levels are normalized by $k_o b$ and 50dB has been added to ensure positive values on all plots. –x-x- $k_o b=0.01$, -o-o-$k_o b=01$, -+-+- $k_o b=1$

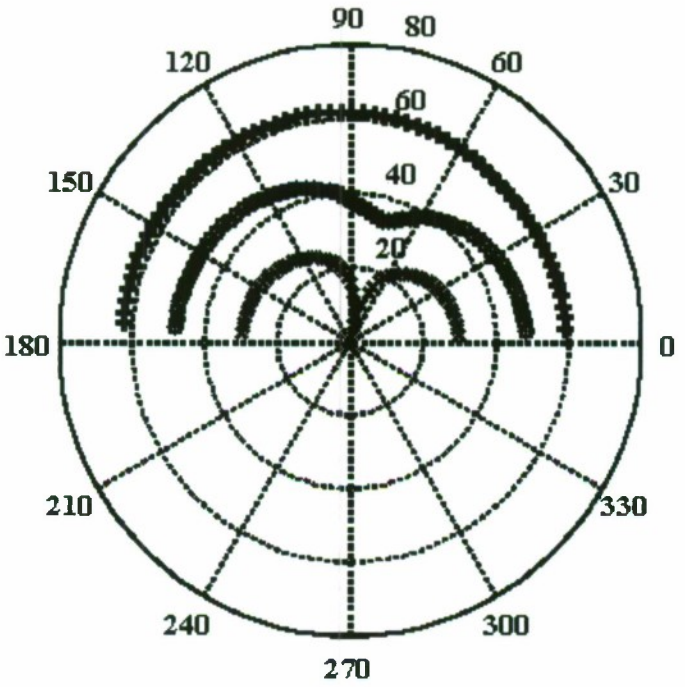


Figure 6: The Directionality of sound from sources near a backward facing step at a Mach number of 0.2. Levels are normalized by $k_o b$ and 50dB has been added to ensure positive values on all plots. –x-x- $k_o b=0.01$, -o-o-$k_o b=01$, -+-+- $k_o b=1$

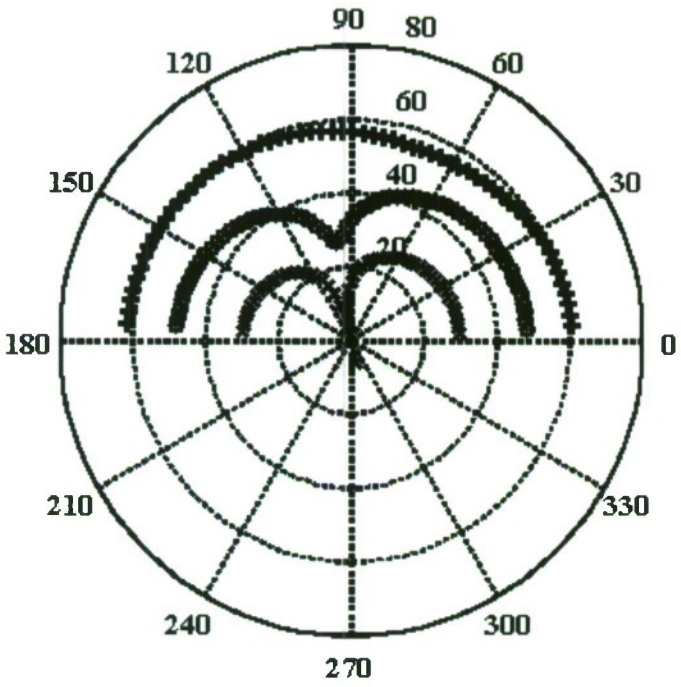


Figure 7: The Directionality of sound from sources near a forward facing step at a Mach number of 0.2. Levels are normalized by $k_o b$ and 50dB has been added to ensure positive values on all plots. –x-x- $k_o b=0.01$, -o-o-$k_o b=01$, -+-+- $k_o b=1$

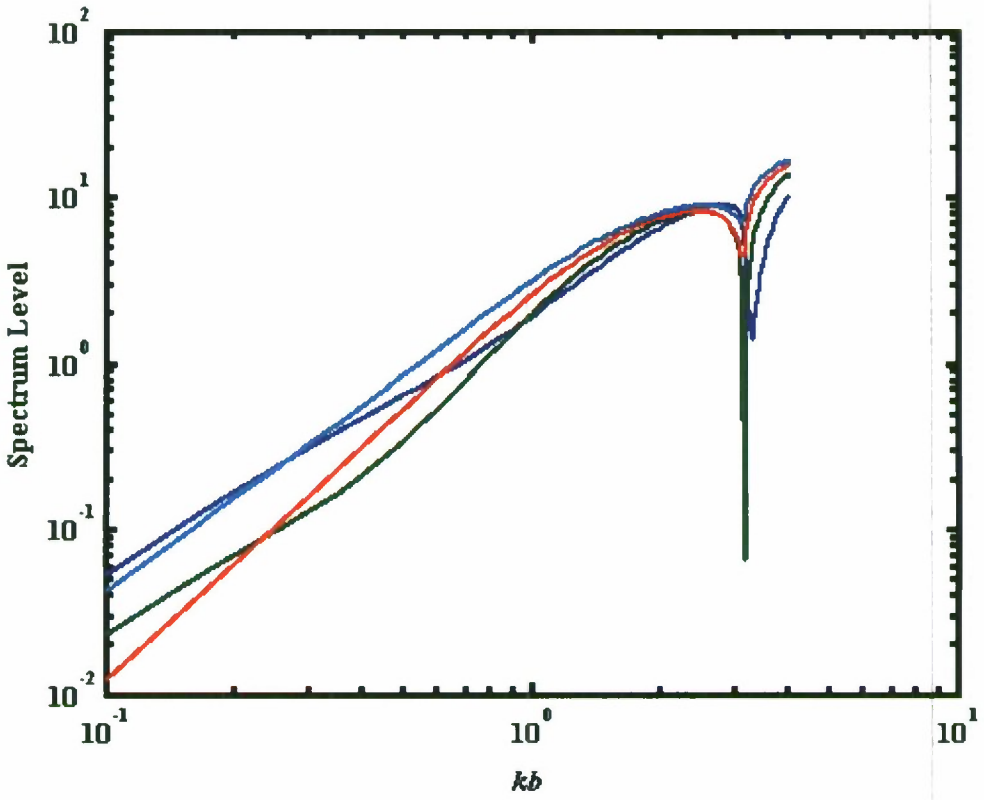


Figure 8: The Greens function as a function of $k_o b$ for a forward facing step at a Mach number of 0.2 at three different angles $\theta$=*56.5°,82.5°,106°*, and *128.5°*

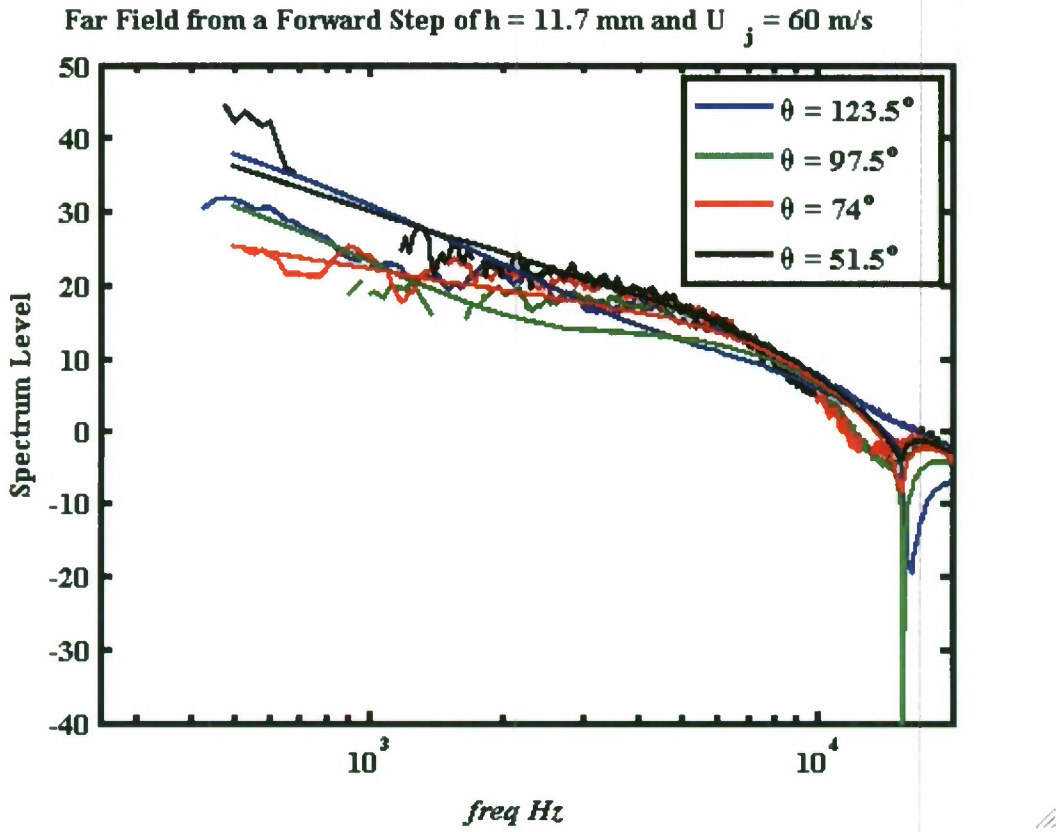


Figure 9: Comparison of measurements by Catlett(2010) and the predictions based on the Greens function developed in this study.

## Part 3: Predictions of Surface Pressure Spectra for a Turbulent Boundary Layer

### 3.1 Introduction

This part of the report will discuss a method for extracting velocity and surface pressure spectra associated with a high Reynolds number turbulent boundary layer. The approach is to develop a description of the turbulent velocity fluctuations based on the solutions to the Orr Sommerfeld and Squire equations and to use these to model the distribution of turbulent stresses within the flow in terms of a set of unknown coefficients. If the distribution of the turbulent stresses is available, either from measurements or RANS calculations, then the model can be inverted to obtain the unknown coefficients and closure is obtained.

This approach has been applied to the flow in a turbulent boundary layer downstream of a forward facing step based on the measurements of Awasthi *et al* 2011. The modeling has identified terms associated with large scale structures in the flow and small scale turbulence, and an energy budget for each term has been obtained as shown in Figure 7. Another output of the model is the turbulent velocity spectra and these are compared to measured spectra at three heights above the wall in Figure 8. The interesting result is that by using the viscous equations with non linear interactions allowed for, the spectra are estimated over a wide range of frequencies without recourse to a modeled turbulence energy spectrum.

### 3.2 Theoretical Background

In the following we will consider methods for evaluating the unsteady part of a fully developed turbulent flow. We will limit consideration to incompressible constant temperature flows and assume that the mean flow is known from a solution to the Reynolds averaged Navier Stokes equations. The flow is defined by its steady velocity and pressure $\mathbf{U}$ and $P$ and its unsteady velocity and pressure $\mathbf{u}$ and $p$. The equation of motion describing the unsteady flow is obtained by subtracting the Reynolds average equation for the steady flow from the full Navier Stokes equations, to give

(1)

$$\frac{\partial \mathbf{u}}{\partial t} + (\mathbf{U}.\nabla)\mathbf{u} + (\mathbf{u}.\nabla)\mathbf{U} + \frac{1}{\rho}\nabla p - \frac{1}{R_e}\nabla^2\mathbf{u} = -\mathbf{b} \qquad \nabla.\mathbf{u} = 0$$

$$\mathbf{b} = (\mathbf{u}.\nabla)\mathbf{u} - \langle(\mathbf{u}.\nabla)\mathbf{u}\rangle$$

The left side of this equation is linear in the unsteady flow variables and the vector $\mathbf{b}$ specifies the contributions from the non linear terms. In the following we will also need a Poisson equation for the pressure, which is obtained in the usual way by taking the divergence of equation (1), and the vorticity equation, which is obtained fro the curl of equation (1)

We will consider velocity perturbations $\mathbf{u}=(u,v,w)$ in a parallel shear flow defined, in Cartesian coordinates $(x,y,z)$ by the mean velocity $U(y)$ in the $x$ direction. The linearized form of the Navier Stokes equations and the continuity equation are used to obtain the Orr Sommerfeld equation (see for example Hallbäck 1996) by taking the Laplacian of (1) for the velocity component in the $y$ direction, subtracting Poissons equation for the pressure, and ignoring the non linear term. However since the non linear terms are important in a fully developed turbulent flow we will retain them here to give an inhomogeneous form of the Orr Sommerfeld equation as

(2)

$$\frac{D_o}{Dt}(\nabla^2 v) - U''\frac{\partial v}{\partial x} - \frac{1}{R_e}\nabla^4 v = -\nabla^2 b_y + (\nabla.\mathbf{b})'$$

where the primes represent differentiation with respect to the $y$ direction, $D_o/Dt=\partial/\partial t+U\partial/\partial x$, and $\mathbf{b}=(b_x,b_y,b_z)$. The $u$ and $w$ components of the velocity can be obtained by considering the vorticity in the $y$ direction, given by $\eta=\partial u/\partial z-\partial w/\partial x$, and the continuity equation (Hallbäck (1996)). The equations for the $u$ and $w$ velocity components are then given in terms of the normal velocity and the normal vorticity as

(3)

$$\frac{\partial^2 u}{\partial x^2}+\frac{\partial^2 u}{\partial z^2} = -\frac{\partial^2 v}{\partial x \partial y}+\frac{\partial \eta}{\partial z} \qquad \frac{\partial^2 w}{\partial x^2}+\frac{\partial^2 w}{\partial z^2} = -\frac{\partial^2 v}{\partial z \partial y}-\frac{\partial \eta}{\partial x}$$

To close this set of equations we use the vorticity equation to obtain an inhomogeneous form of Squires equation for the normal component of the vorticity as

(4)

$$\frac{D_o \eta}{Dt} - \frac{1}{R_e}\nabla^2 \eta + U'\frac{\partial v}{\partial z} = -\nabla \times \mathbf{b}$$

These homogeneous form of these equations have been considered by many different authors (see for example Drazin and Reid(1981), Hallbäck (1996) for reviews) to investigate flow instabilities and boundary layer transition. Solutions have been sought that identify the growth or decay of disturbances and it can be shown that, in the inviscid case, the amplitude of the normal component of the velocity grows linearly with time from an initial disturbance. Also it can be shown that a boundary layer flow will be unstable if the mean velocity profile includes a point of inflexion. However in this study we are interested in using linear theory to describe a high Reynolds number fully developed turbulent flow, which is characterized as stationary in time and homogeneous in the $x$ and $z$ directions. On this basis we will seek solutions in the frequency/wavenumber domain by considering the Fourier transform of all variables, defined as

(5)

$$\hat{f}(y,\omega,\alpha,\beta) = \frac{1}{(2\pi)^3}\int_{-T}^{T}\int_{-R}^{R}\int_{-R}^{R} f(x,y,z,t)e^{-i\omega t - i\alpha x - i\beta z}dxdzdt$$

Taking the Fourier transform of the inhomogeneous Orr Sommerfeld and Squire equations then gives

(6)

$$(\alpha U+\omega)(\hat{v}''-\lambda^2\hat{v})-\alpha U''\hat{v}-\frac{i}{R_e}(\hat{v}''''-2\lambda^2\hat{v}''+\lambda^4\hat{v})=\hat{B}$$

$$(\alpha U+\omega)\hat{\eta}+\beta U'\hat{v}-\frac{i}{R_e}(\hat{\eta}''-\lambda^2\hat{\eta})=\hat{C}$$

$$\lambda^2=\alpha^2+\beta^2 \qquad \hat{B}=i\lambda^2\hat{b}_y+\alpha\hat{b}_x'+\beta\hat{b}_z' \qquad C=-\beta\hat{b}_x+\alpha\hat{b}_z$$

and the $u$ and $w$ components of the velocity are defined as

(7)

$$\hat{u}=\frac{-i(\alpha\hat{v}'-\beta\hat{\eta})}{\lambda^2} \qquad \hat{w}=\frac{-i(\beta\hat{v}'+\alpha\hat{\eta})}{\lambda^2}$$

This provides a closed set of equations which may be solved to obtain all the velocity components of the flow in terms of the unknown functions $\hat{B}$ and $\hat{C}$. We will start by solving for the normal velocity, which can be considered independently, and then consider the normal vorticity, which depends on the distribution of normal velocity. With these two results we can then obtain the velocity components parallel to the mean flow given by equation (7).

### 3.3 The Normal Velocity

In order to solve equation (6) we need to specify the details of the mean velocity profile in the boundary layer. This has a discontinuity in its slope at the interface between the viscous sublayer and the log layer, and so we will treat the viscous sublayer and the log layer as separate regions. In the viscous sublayer the non linear terms on the right of equation (6) can be considered small compared to the viscous terms, and the velocity profile is linear, so the equation (6) reduces to its homogeneous form and will depend on the boundary conditions on the surface and at the interface with the log layer. The OS equation is of fourth order and so four boundary conditions will be required to specify the flow in the viscous sublayer. These are that $v$ and $v'$ should be zero on the surface, and the $v$ and $v'$ should be continuous across the interface with the log layer where $y=y_s$.

In the log layer we will seek a solution using the Greens function for the OS equation which is the solution to

(8)

$$(\alpha U+\omega)(G''-\lambda^2 G)-\alpha U''G-\frac{i}{R_e}(G''''-2\lambda^2 G''+\lambda^4 G)=\delta(y-y_1)$$

and satisfies the same boundary conditions as $\hat{v}$ at $y=y_s$ and at infinity. Giving the normal velocity as

(9)

$$\hat{v}(y)=\int_{y_s}^{\infty}\hat{B}(y_1)G(y\,|\,y_1)dy_1$$

### 3.4 The Normal Vorticity

The solution for the normal vorticity is obtained using the same approach as above. From the second equation in (6) we obtain

(10)

$$\hat{\eta} = \int_{y_s}^{\infty} (\hat{C} - \beta U'(y_1)\hat{v}(y_1)) G_\eta(y \mid y_1) dy_1$$

where $G_\eta$ is the Greens function that satisfies the equation

(11)

$$(\omega + \alpha U) G_\eta(y \mid y_1) - \frac{i}{R_e}(G_\eta''(y \mid y_1) - \lambda^2 G_\eta(y \mid y_1)) = \delta(y - y_1)$$

In this case there are two contributing source terms. The first is from the non linear term $\hat{C}$ that acts as a source of normal vorticity and the second is from the interaction term associated with the normal velocity. We can combine equations (9) and (11) for the interaction term to give

(12)

$$\hat{\eta}_v = -\int_{y_s}^{\infty} \hat{B}(y_2) G_v(y \mid y_2) dy_2$$

$$G_v(y \mid y_2) = \left\{ \int_{y_s}^{\infty} \beta U'(y_1) G_\eta(y \mid y_1) G(y_1 \mid y_2) dy_1 \right\}$$

### 3.5 The Greens Functions

The Greens functions defined above are shown in figures 1-3 for different frequencies and wavenumbers. In all cases the spatial resolution was set as *dy=1/500* and the number of terms in the Fourier series expansion limited to 50. The boundary layer mean velocity profile was given by $U=y^{1/7}$, and the Reynolds number was $5 \times 10^5$.

In figure 1 the Greens function for the OS equation and the interaction term are compared for a non dimensional frequency of $\omega=1$ and wavenumbers $\alpha=-1.285$ and $\beta=1$. It is seen that the impact of a source term (in this case the non linear term *B*) at any location $y_1$ has a non local impact on the flow, which indicates the possibility of a large scale structure. We note that at this frequency the interaction term that drives the normal vorticity is of a much lower level than than the Greens function driving the normal velocity. However at lower frequencies as shown in figure 2, the interaction term dominates.

In figure 3 we show the Greens function for Squires equation that shows how the normal vorticity is driven by the non linear source term *C*. In this case we see that there is only a local reaction, and the impact of the source term is very local. This implies that this term is responsible for the small scale turbulence in the flow and is not associated with large scale structures.

### 3.5 Large scale Structures and Small Scale Turbulence

In the previous section it was shown that the unsteady part of the Reynolds average equations can be solved by assuming that the non linear terms are small and act as sources of disturbance to the larger linear terms. By evaluation the solutions to these equations it was found that there are two components driving the flow, one that has a broad non local impact and another that only impacts the flow locally. In the following we will consider these two different terms as representing the large scale structures in the flow and the small scale turbulence. The small scale turbulence only couples with the vorticity normal to the wall and only has velocity components parallel to the wall. In contrast the large scale structures have velocity and vorticity components in all three directions.

We will assume that the flow may be broken down into large scale structures and small scale turbulence, and that the large scale structures propagate with their own phase speed $c_k$ and that the non linear terms associated with each structure can be superposed such that

$$B(t,x,y,z)=\sum_{k=1}^{K} A_k B_k(t-x/c_k,y,z) \tag{13}$$

where $0<c_k<1$, $A_k$ represents the amplitude of the structure and $B_k(t,y,z)$ is the distribution of the non linear terms for the large scale structure of order $k$. Using this model we can define the source terms in equation (6) as

$$\hat{B}(y,\omega,\alpha,\beta)=\sum_{k=1}^{K} A_k \hat{B}_k(y,\omega,\beta)\delta(\alpha+\omega/c_k) \tag{14}$$

and it follows that the normal velocity is given by

$$v(\mathbf{x},t)=\int_{-\infty}^{\infty}\int_{-\infty}^{\infty}\sum_{k=1}^{K} A_k v_k(y,\omega,\beta)e^{-i\omega(t-x/c_k)-i\beta z}d\omega d\beta \tag{15}$$

where

$$v_k(y,\omega,\beta)=\int_{y_s}^{R} \hat{B}_k(y_1,\omega,\beta)\left[G(y\,|\,y_1\right]_{\alpha=-\omega/c_k} dy_1 \tag{16}$$

Similar expression can be obtained for $\eta_v$ and the velocity components $u$ and $w$ by utilizing equation (12) and (7).

Summarizing the results gives the velocity field as

$$\mathbf{u}(\mathbf{x},t)=\sum_{k=1}^{K} A_k \mathbf{u}_k(t-x/c_k,y,z)+\mathbf{u}_s(t,x,y,z) \tag{17}$$

where $\mathbf{u}_k$ is the velocity perturbation associated with each large scale structure and $\mathbf{u}_s$ is the velocity of the small scale turbulence, and we can define

(18)

$$\mathbf{u}_k(\mathbf{x},t) = \int_{-\infty}^{\infty}\int_{-\infty}^{\infty} \hat{\mathbf{u}}_k(y,\omega,\beta)e^{-i\omega(t-x/c_k)-i\beta z}d\omega d\beta$$

$$\mathbf{u}_s(\mathbf{x},t) = \int_{-\infty}^{\infty}\int_{-\infty}^{\infty}\int_{-\infty}^{\infty} \hat{\mathbf{u}}_s(y,\omega,\alpha,\beta)e^{-i\omega t-i\alpha x-i\beta z}d\omega d\alpha d\beta$$

where

(19)

$$\hat{\mathbf{u}}_k = (\hat{u}_k,\hat{v}_k,\hat{w}_k) \qquad \hat{u}_k = \left[\frac{-i(\alpha\hat{v}_k' - \beta\hat{\eta}_k)}{\lambda^2}\right]_{\alpha=-\omega/c_k} \qquad \hat{w}_k = \left[\frac{-i(\beta\hat{v}_k' + \alpha\hat{\eta}_k)}{\lambda^2}\right]_{\alpha=-\omega/c_k}$$

with

(20)

$$\eta_k(y,\omega,\beta) = -\int_{y_s}^{R} \hat{B}_k(y_1,\omega,\beta)\left[G_v(y\,|\,y_1\right]_{\alpha=-\omega/c_k} dy_1$$

and for the small scale turbulence

(21)

$$\hat{\mathbf{u}}_s = (\hat{u}_s,0,\hat{w}_s) \qquad \hat{u}_s = \left[\frac{i\beta\hat{\eta}_s}{\lambda^2}\right]_{\alpha=-\omega/c_k} \qquad \hat{w}_s = \left[\frac{-i\alpha\hat{\eta}_s}{\lambda^2}\right]_{\alpha=-\omega/c_k} \qquad \hat{\eta}_s = \int_{y_s}^{\infty} \hat{C}(y_1)G_\eta(y\,|\,y_1)dy_1$$

An example of the velocities associated with a large scale structure is given in Figure 4 where it is seen that at this frequency and wavenumber all three components are of similar magnitude. At lower frequencies the normal velocity is relatively smaller, and at higher frequencies the normal velocity dominates the result.

### 3.6 Modeling the Non Linear Terms and Statistical Averages

#### 3.6.1 Non Linear Terms

The non linear terms in the above analysis are unknown and so we must resort to some type of modeling to approximately account for their characteristics. The non linear terms may be both sources and sinks of energy and we must delineate between these effects. The reduction of energy in the flow can be modeled in the same way that we model non linear turbulent flow terms in the steady RANS equations, by introducing an eddy viscosity of the viscous term on the left of the OS equation and Squires equation. The sources, or production terms, remain on the right and it is these that we will model here.

We will assume that the non linear terms are dominated by the small scale turbulence, which feeds the large scale structure, and model the non linear term as

$$\hat{B}_k = \omega^{n_1}\beta^{n_2} |G_\eta(y,y_k)/G_\eta(y_k,y_k)|^2 \tag{22}$$

where $n_1$ and $n_2$ are modeling coefficients, which are found to be $n_1=n_2=2$ from comparison with experimental data.

### 3.6.2 The Turbulent Kinetic Energy

For the large scale structure modes we can define the turbulent stresses at the location $y$ by averaging velocity at a fixed point. Since the flow is statistically stationary in time and homogeneous in $x$ and $y$, different frequencies, wavenumbers and modes must be uncorrelated and we obtain

$$\sigma_{vv}(y) = E[|v(\mathbf{x},t)|^2] = \int_{-\infty}^{\infty}\int_{-\infty}^{\infty}\sum_{k=1}^{K} A_k^2 |v_k(y,\omega,\beta)|^2 \, d\omega d\beta \tag{23}$$

Similar expression can be defined for the other velocity components and the turbulent kinetic energy for the large scale structures is given by

$$\kappa_o(y) = \frac{1}{2}\int_{-\infty}^{\infty}\int_{-\infty}^{\infty}\sum_{k=1}^{K} A_k^2\left(|u_k(y,\omega,\beta)|^2 + |v_k(y,\omega,\beta)|^2 + |w_k(y,\omega,\beta)|^2\right) d\omega d\beta \tag{24}$$

The total kinetic energy is then given by

$$\kappa(y) = \kappa_o(y) + \kappa_s(y) \tag{25}$$

where $\kappa_s$ is the kinetic energy of the small scale structures.

Similarly the spectrum of the velocity fluctuations is given by

$$S_{vv}(\omega,y) = \int_{-\infty}^{\infty}\sum_{k=1}^{K} A_k^2 |v_k(y,\omega,\beta)|^2 \, d\beta \tag{26}$$

To evaluate these expressions we need to accurately integrate over the wavenumber $\beta$. We can show that all terms in the integral are a function of $\beta^2$ and so the integrals can be carried out over the half range $0<\beta<\infty$. Furthermore to reduce the computational effort we can use logarithmic steps in wavenumber to extend the integration over a wider range of wavenumbers for a given number of computations.

### 3.6.3 Surface Pressure Spectra

The surface pressure spectrum can be calculated from the solution to Poissons equation

(27)

$$\hat{p}'' - \lambda^2 \hat{p} = i\rho\alpha\hat{v}U' - \rho\nabla.\mathbf{b}$$

It is argued that the linear term will be of order $U/u$ larger than the non linear term on the right side of this equation, and since this is directly proportional to the normal velocity, it follows that the surface pressure is determined exclusively by the large scale structures in the flow because the small scale turbulence is parallel to the mean flow. This has important modeling implications because it implies that the convection speed of the large scale structures vary from near zero to the outer stream velocity. However it does not relate the scale of the large scale structure to its convection speed because nothing has been assumed about the scale of the structure in the $x$ direction.

To obtain the surface pressure we first need to solve equation (27) subject to the boundary condition that $p'=0$ on $y=0$. If the non linear tem is ignored in comparison with the linear term then we obtain

(28)

$$\hat{p}(y) = \frac{-1}{2\lambda}\int_0^\infty i\rho\alpha U'(y_1)\hat{v}(y_1)(e^{-\lambda|y-y_1|} + e^{-\lambda(y+y_1)})dy_1$$

Then using the expansion in equations (17-19) the surface pressure becomes

(29)

$$p(t) = \sum_{k=1}^{\infty} A_k \int_{-\infty}^{\infty}\int_{-\infty}^{\infty}\left[\frac{-i\rho\alpha}{\lambda}\int_0^\infty U'(y_1)v_k(y_1)e^{-\lambda y_1}\right]_{\alpha=-\omega/c_k} e^{-i\omega t}dy_1 d\beta d\omega$$

These results can also be used to calculate the frequency spectrum of the surface pressure fluctuations. Since the modes are uncorrelated this is defined as

(30)

$$S_{pp}(\omega) = \sum_{k=1}^{\infty} A_k^2 \int_{-\infty}^{\infty}\left|\left[\frac{\rho\alpha}{\lambda}\int_0^\infty U'(y_1)v_k(y_1)e^{-\lambda y_1}dy_1\right]_{\alpha=-\omega/c_k}\right|^2 d\beta$$

### 3.7 Comparison with Experimental Results

The model given here was compared to experimental measurements made in the stability wind tunnel at Virginia Tech, as reported Awasthi et al (2011). We will present results for a fully developed turbulent boundary layer with a Reynolds number of $1.73\text{x}10^5$. The mean velocity profile and the turbulent stresses as a function of displacement from the wall are shown in figure 5. To compare the measurements to the theoretical model we still need to define the unknown coefficients $A_k$. To find these we can use equation (23) for the normal turbulent stress and use a least squares algorithm to fit the data to the model. The algorithm must be constrained so that $A_k^2>0$ and the number of coefficients must be less than the number of measurements points to obtain a converged result. Figure 6 shows the amplitude of each structure verses mode order $k$, and it is seen that the energy is distributed across the modes and no one mode dominates. The strongest contribution is from mode order 2, but this is only a factor of 2 above the other modes.

With these coefficients we can now estimate the turbulent kinetic energy (tke) from the large scale structures using equation (24). The result is shown in figure 7 and is compared to the measured tke. The difference is attributed to the tke from the small scale structures and this is also shown in figure 7. The result indicates that the energy is the small scale structures dominates the tke budget by a factor of about two.

As an independent check on the validity of the results we can also calculate the spectrum of the normal velocity using equation (26) and this is compared to the measured results in figure 8 at three different locations in the boundary layer. The spectral shape appears to be well modeled by this approach, and is an interesting result because no spectral modeling or lengthscales have been required to make this calculation.

The prediction of the unsteady flow have also been applied to a boundary layer downstream of a forward facing step as measured by Awasthi et al (2011). Figure 9 shows the boundary layer profile and the distributions of turbulent stresses at nine step heights downstream of the step. The profiles are distinctly different from those for the undisturbed boundary layer shown in figure 5. The breakdown of the tke between small and large scale turbulence is shown in figure 10, and this is clearly dominated by the large scale structure tke as distinct from the small scale tke. This gives an important contrast to the results for the undisturbed boundary layer that was dominated by the small scale tke. In figure 11 the spectra of the vertical velocity fluctuations is given at three different heights in the boundary layer. In this case the spectra show significant level differences at different locations across the boundary layer, and the theory follows the trend in the measurements, as well as providing the spectral shape. In contrast the results for the boundary layer 36 step heights downstream of the step (figure 12) show that the vertical velocity spectra are similar at all locations, similar to the undisturbed boundary layer.

Finally in figure 13 we show the estimates of the surface pressure spectra for the undisturbed boundary layer, and the boundary layer at 9 and 36 step heights downstream of the step. Given the good predictions of the vertical velocity one might expect the surface pressure spectra to be well predicted as well, given the relationship specified by equation (30). However the only reasonable prediction is for the undisturbed boundary layer at low frequencies. However, the analysis given here, and the measurements have only included the turbulence in the outer part of the boundary layer and have not considered the viscous sublayer and the log law region, which are closest to the wall and will dominated the terms in equation (30). It is not surprising therefore that the predicted surface pressure spectra, that are dominated by near wall effects, are not well predicted by this method.

### 3.8 Conclusions

In this study we have made use of the unsteady part of the RANS equations to model the flow in a boundary and downstream of a forward facing step. It has been shown that the flow can be broken down into large and small scale turbulence. The large scale turbulent structures are convected at their own fixed speed, while the small scale turbulence is uncorrelated from point to point in the vertical direction, and convected at the local flow speed. The energy balance between these two mechanisms is dominated by the small scale turbulence for the undisturbed

boundary layer, but in the case of the flow down stream of a step results are quite different. At 9 step heights downstream of the step the large scale turbulence dominates, indicating that the disturbances generated by the step are dominating the flow.

While the estimates of the vertical velocity compare well with the measurements, the surface pressure spectra at different locations downstream of the step are not as well estimated. The explanation for this is that the model has not included the inner layers where the turbulent structures are expected to dominate the surface pressure fluctuations.

**References**


Awasthi M., Forest J. B., Morton M. A., Devenport W., Glegg S., 2011, "The Disturbance of a High Reynolds Number Turbulent Boundary Layer by Small Forward Steps", 17th AIAA/CEAS Aeroacoustics Conference, June 6th-8th, Portland OR, AIAA-2011-2777

Devenport W J, Muthanna C and Glegg S A L, (2001), "Two-Point Descriptions of Wake Turbulence with Application to Noise Prediction", AIAA Journal, vol. 39, no. 12, pp. 2302-2307

S.Glegg, B.Morin, O. Atassi, and R.Reba "Using RANS calculations to provide predictions of trailing edge noise" *AIAA. AIAA JOURNAL.* Vol. 48, No. 7, July 2010

Hallbäck, M. , 1996, Turbulence and Transition Modeling, Springer, 1996, Chapter 2 (lecture notes from the ERCOFTAC/IUTAM summer school held in Stockholm, 12-20 June, 1995).

Lee, Y-T, Blake, W.K., Farabee, T.M., (2005), "Modeling of wall pressure fluctuations based on time mean flow field" , Journal of Fluids Engineering, Vol 127, pp233-240

Hallback, M., Henningson, D.S., Johansson, A.V., and Alfredsson, P.H., 1996, Turbulence and transition modeling, Kluwer Academic Publishers

Drazin, P.G., and Reid, W.H., 1981 Hydrodynamic Stability, 2nd edition, Cambridge

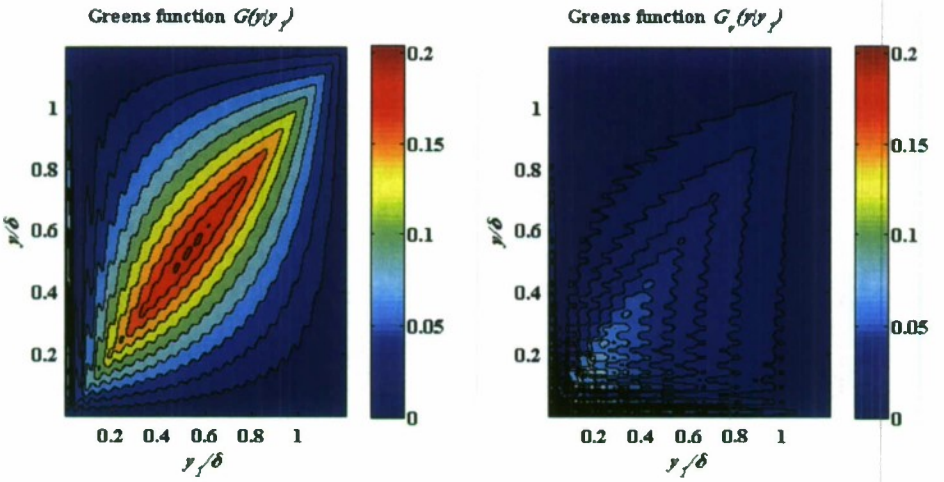


Figure 1: The Greens functions for a boundary layer flow at a Reynolds number of $5x10^5$, frequency $\omega$=1 and wavenumbers $\alpha$=*-1.285*,$\beta$=1. Left figure is the Greens function for the OS equation, right figure is the interaction Greens function defined by equation (12).

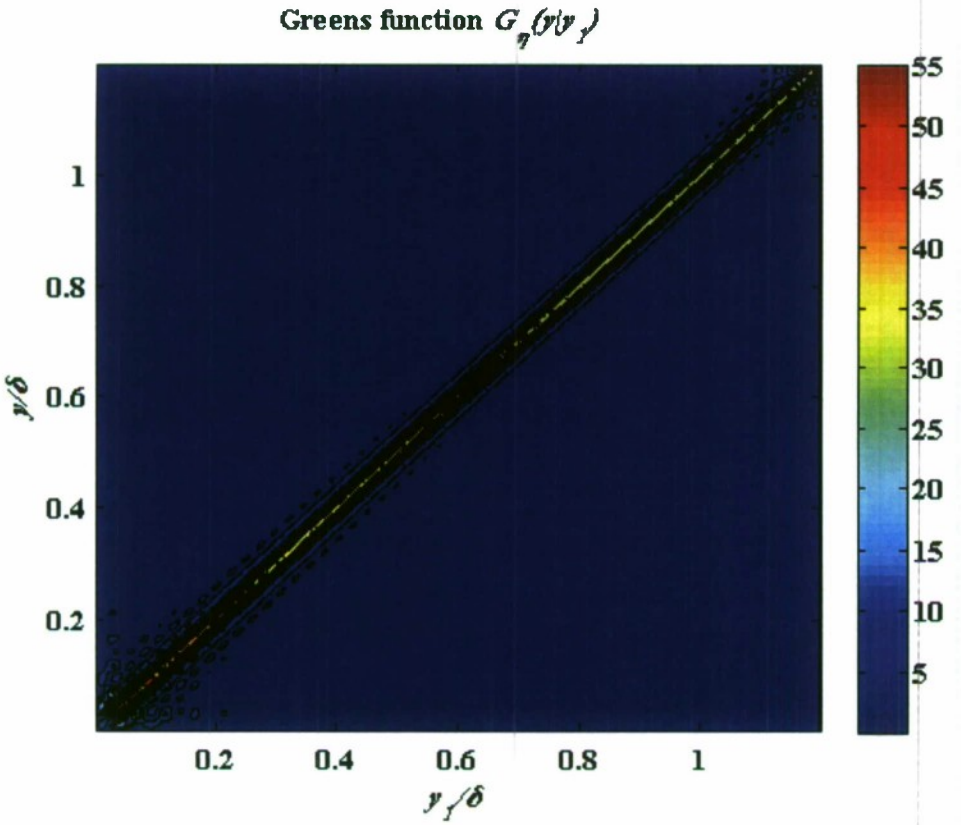


Figure 2: The Greens function for Squires equation for a boundary layer flow at a Reynolds number of $5x10^5$, frequency $\omega$=1 and wavenumbers $\alpha$=*-1.285*,$\beta$=1.

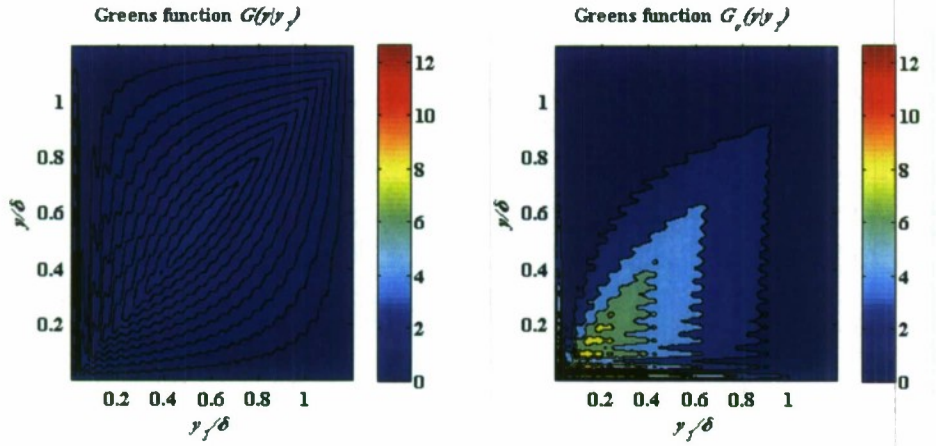


Figure 3: The Greens functions for a boundary layer flow at a Reynolds number of $5x10^5$, frequency $\omega$=0.1 and wavenumbers $\alpha$=-0.1285,$\beta$=1. Left figure is the Greens function for the OS equation, right figure is the interaction Greens function defined by equation (12).

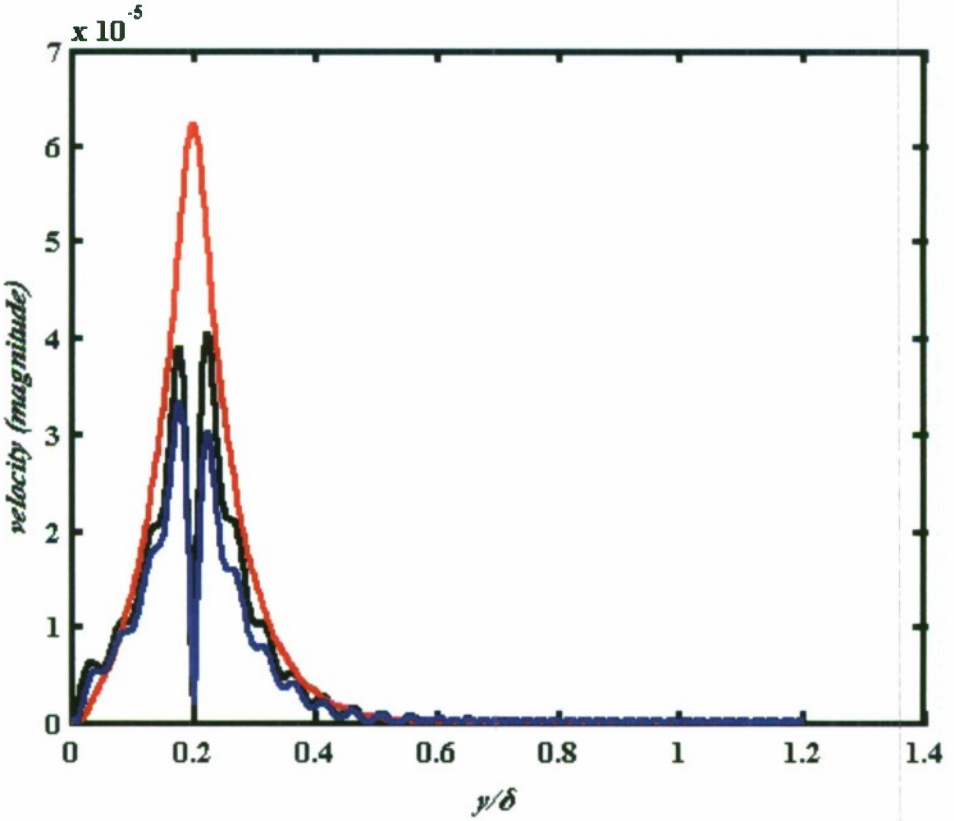


Figure 4: The three velocity components for a large scale structure at $\omega$=10,$\alpha$=-12.85, $\beta$=10 red is $v$, black is $u$, blue is $w$

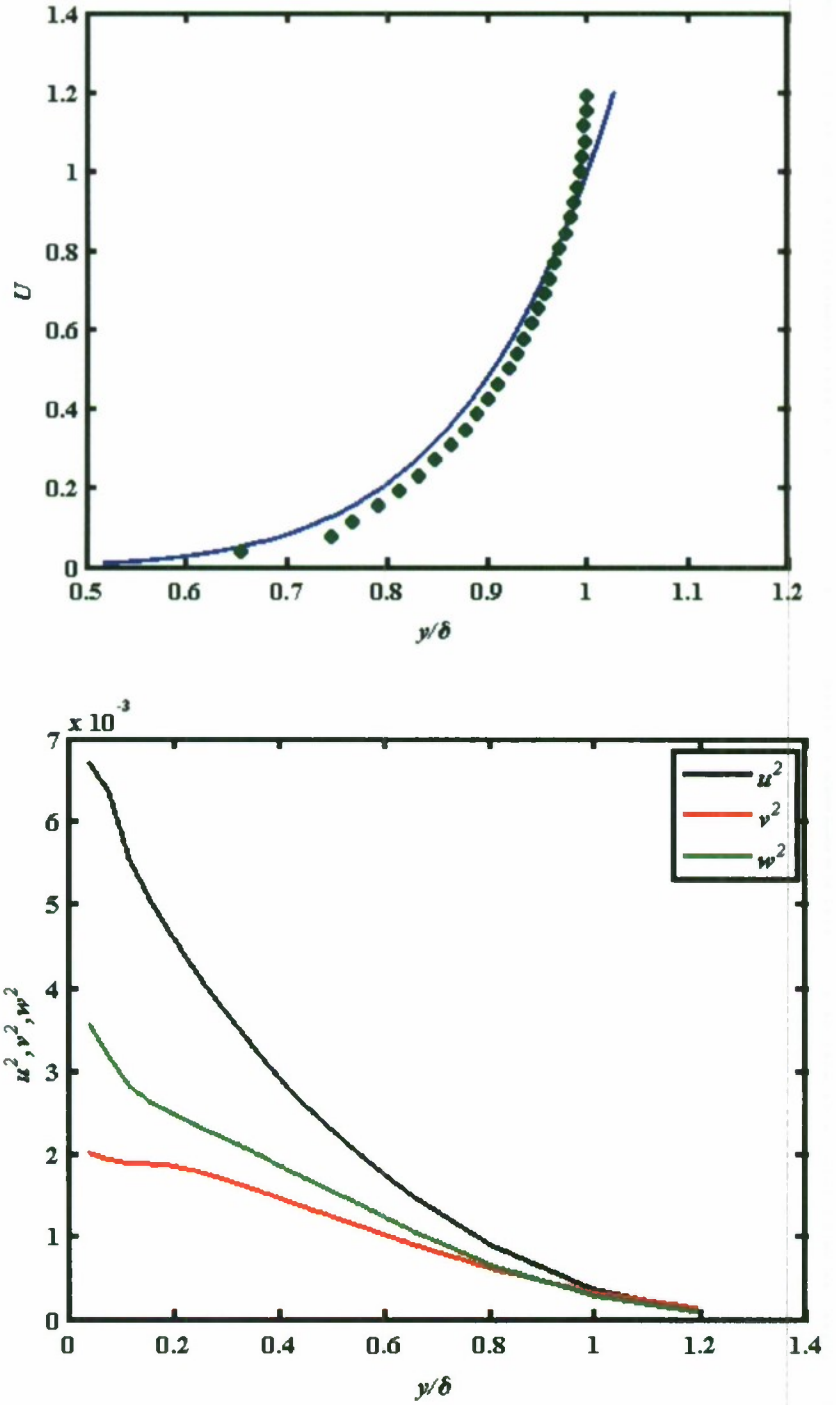


Figure 5: The upper figure shows the boundary layer mean velocity profile measured in the VT Stability wind tunnel at a Reynolds number of $1.73 \times 10^5$ . the lower figure shows the measured turbulent stresses. Red is $v^2$, green is $w^2$ and black is $u^2$.

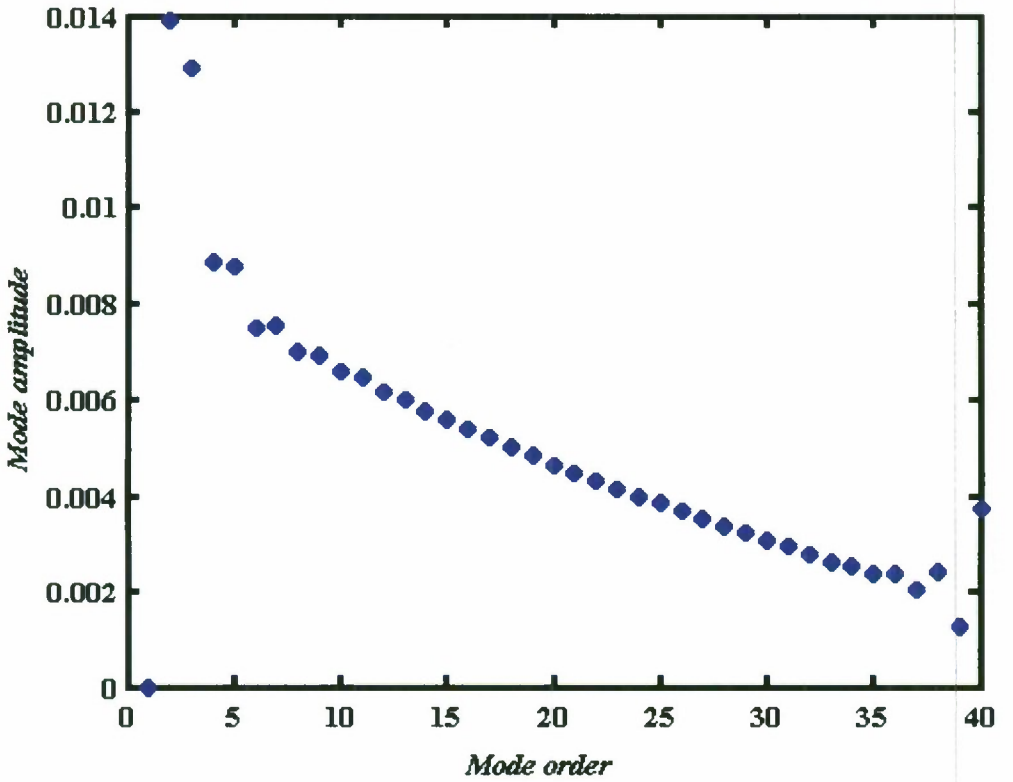


Figure 6: The velocity mode amplitudes for a boundary layer flow at a Reynolds number of $1.73 \times 10^5$.

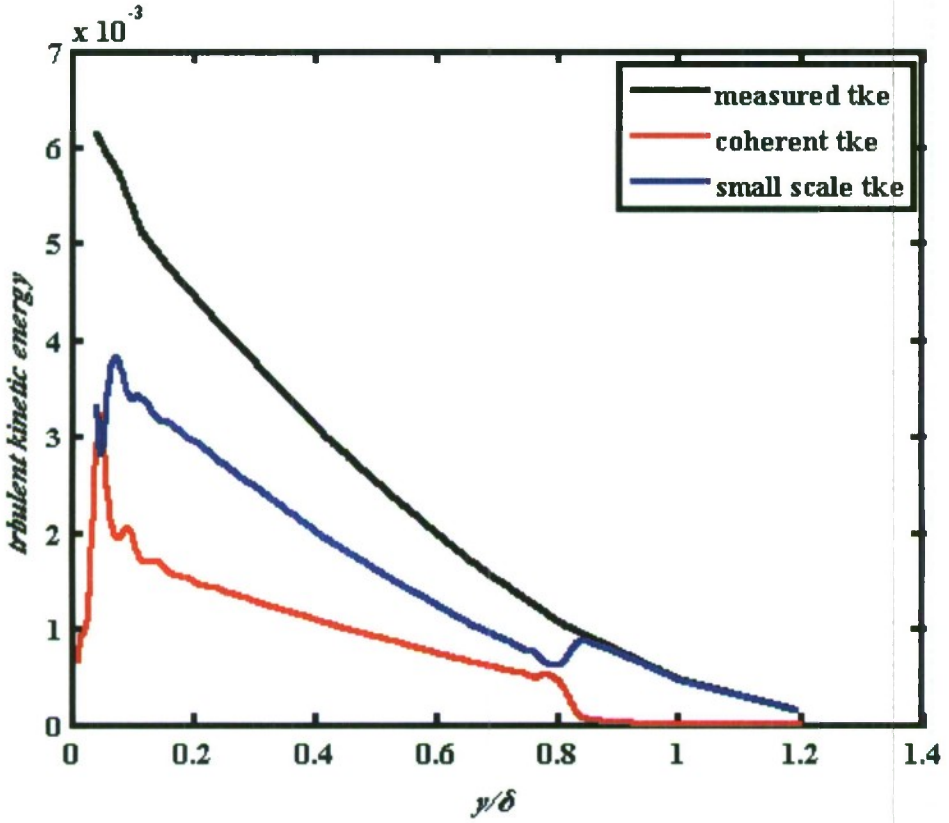


Figure 7: The turbulent kinetic energy budget for a boundary layer flow at a Reynolds number of $5x10^5$ showing the breakdown between the energy in the large scale structures and small scale turbulence.

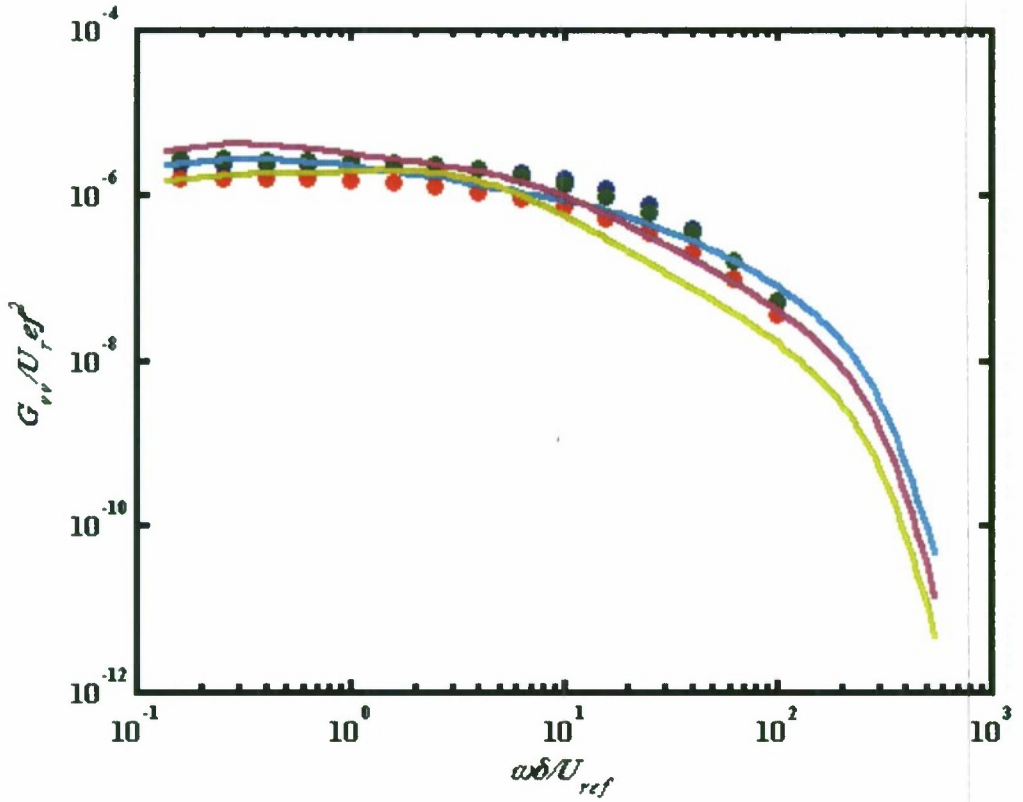


Figure 8: The normal velocity spectra for a boundary layer flow at a Reynolds number of $1.73 \times 10^5$ at three different location in the boundary layer. Lines are experimental measurements and dots are the model estimates.

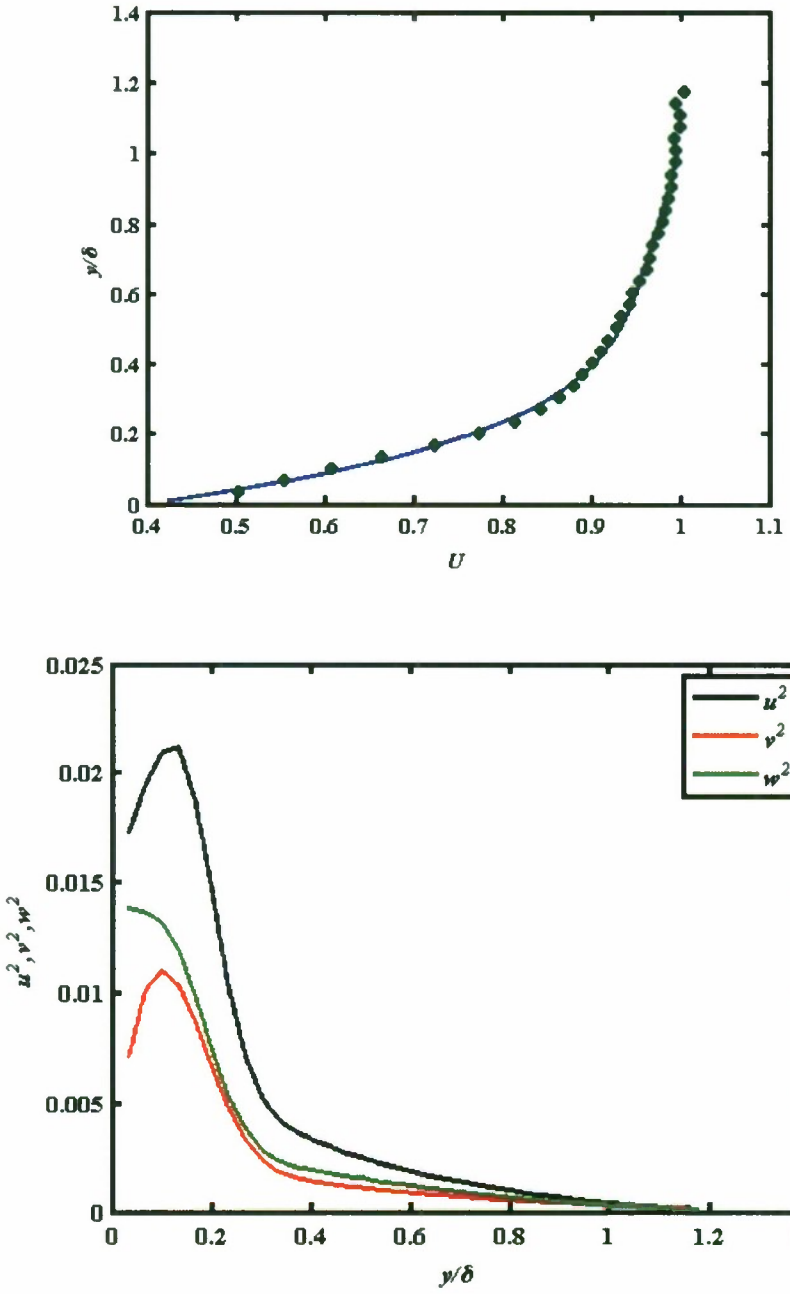


Figure 9: The upper figure shows the boundary layer mean velocity profile measured in the VT Stability wind tunnel 9 step heights downstream of a forward facing step, at a Reynolds number of $1.73 \times 10^5$ . The lower figure shows the measured turbulent stresses. Red is $v^2$, green is $w^2$ and black is $u^2$.

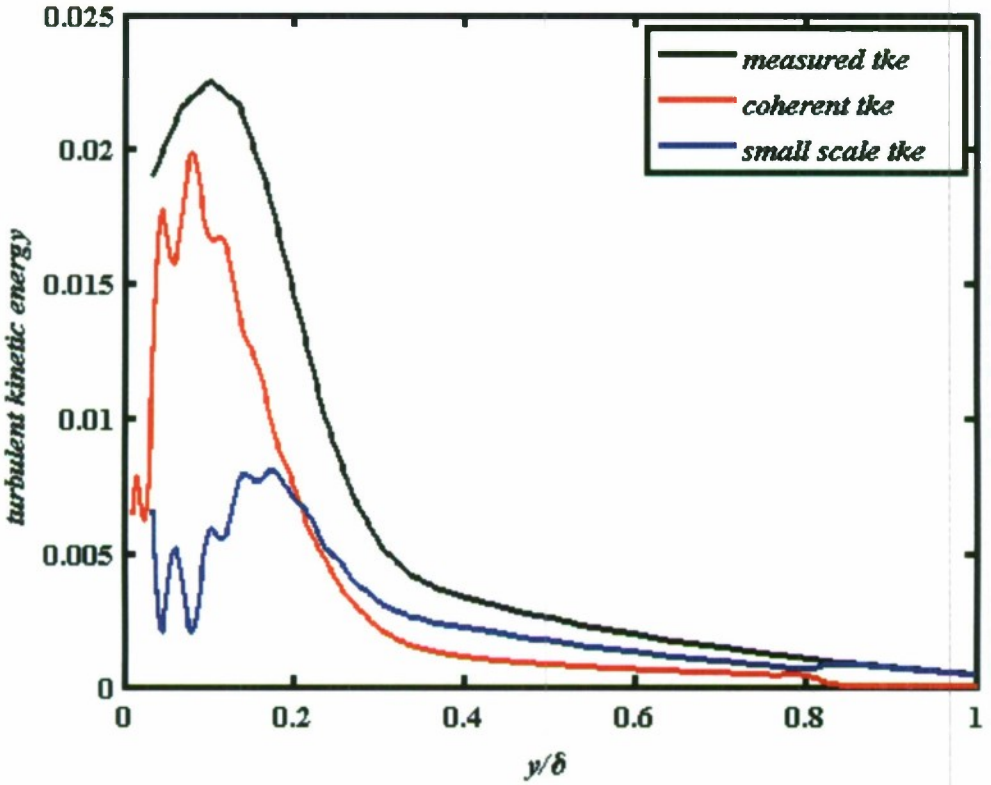


Figure 10: The turbulent kinetic energy budget for a boundary layer flow 9 step heights downstream of a forward facing step at a Reynolds number of $1.73 \times 10^5$ showing the breakdown between the energy in the large scale structures and small scale turbulence.

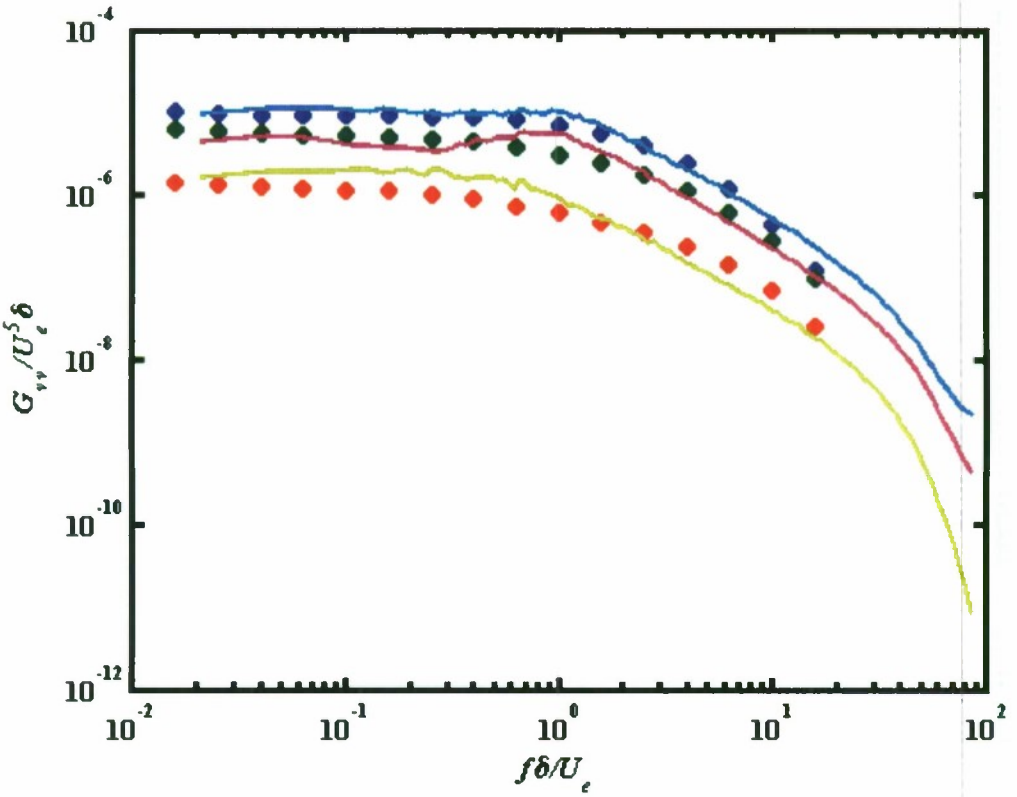


Figure 11: The normal velocity spectra for a boundary layer flow 9 step heights downstream of a forward facing step at a Reynolds number of $1.73 \times 10^5$ at three different location in the boundary layer, $y/\delta = 0.0672, 0.2353, 0.5379$. Lines are experimental measurements and dots are the model estimates.

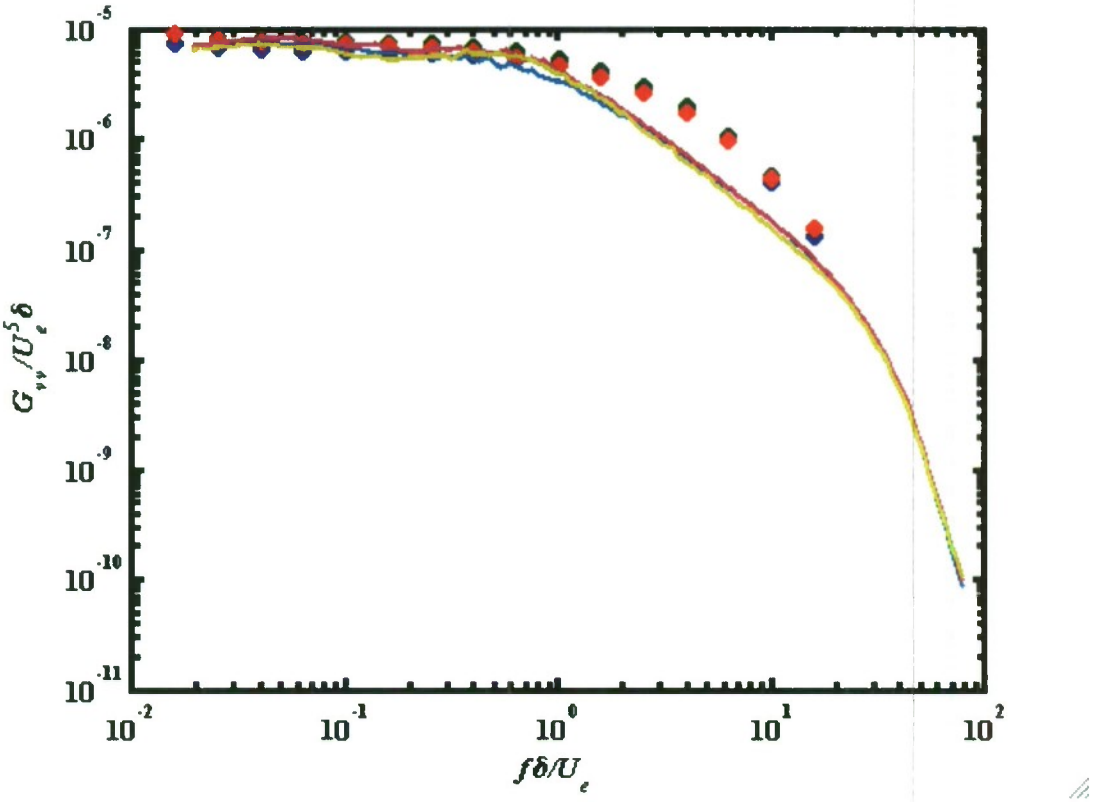


Figure 12: The normal velocity spectra for a boundary layer flow 36 step heights downstream of a forward facing step at a Reynolds number of $1.73 \times 10^5$ at three different location in the boundary layer, $y/\delta = 0.0672, 0.2353, 0.5379$. Lines are experimental measurements and dots are the model estimates.

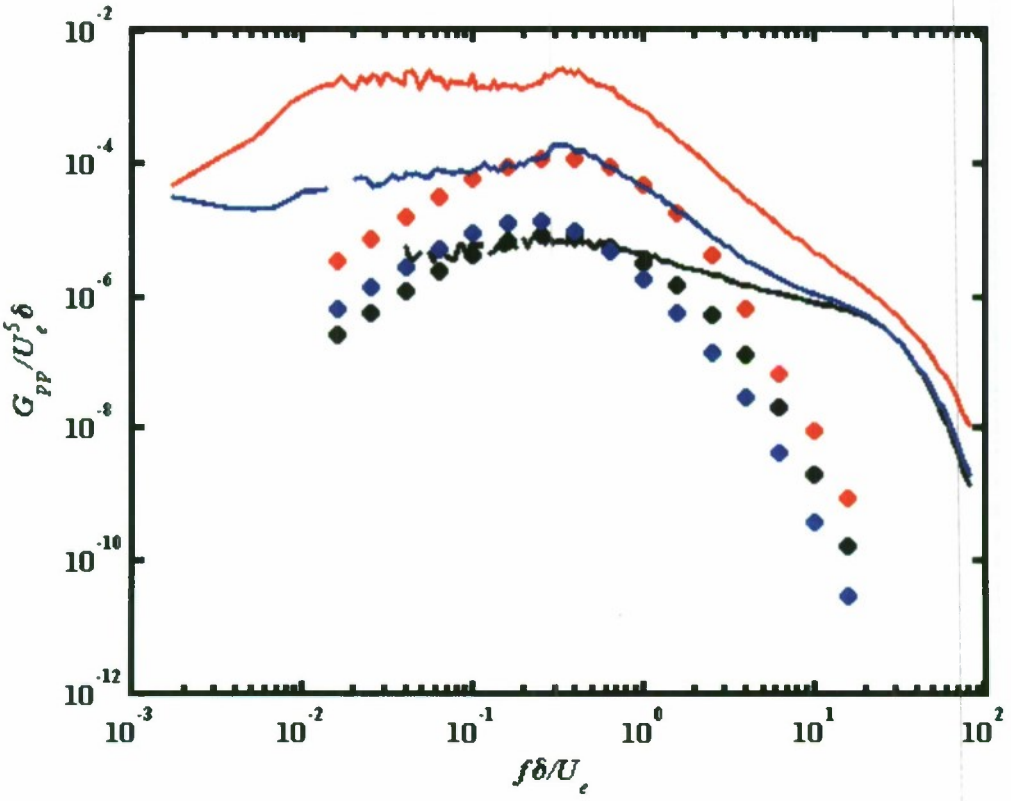


Figure 13: The surface pressure spectra for a boundary layer flow. Black line (measurements) and (predictions) dots are for the undisturbed boundary layer, blue line (measurements) and (predictions) dots are at 9 step heights downstream of a forward facing step, and red line (measurements) and (predictions) dots are at 36 step heights downstream. All cases are at a Reynolds number of $1.73 \times 10^5$ at three different location in the boundary layer, $y/\delta = 0.0672, 0.2353, 0.5379$.